HELSINGIN YLIOPISTO
HELSINGFORS UNIVERSITET
UNIVERSITY OF HELSINKI

Master`s thesis
Department of Geosciences and Geography
Geology

Inferences of magma interaction processes from mineral chemistry and geothermobarometry of mingled and mixed rock types in the Ahvenisto complex, SE Finland

Hanna-Kaisa Ruhanen
May 2022

UNIVERSITY OF HELSINKI
FACULTY OF SCIENCE

P.O. Box 64 (Gustaf Hällströmin katu 2)
FI-00014 University of Helsinki
Finland

HELSINGIN YLIOPISTO
HELSINGFORS UNIVERSITET
UNIVERSITY OF HELSINKI

Tiedekunta/Osasto Fakultet/Sektion – Faculty	Laitos/Institution– Department
Faculty of Science	Department of Geosciences and Geography

Tekijä/Författare – Author

Hanna-Kaisa Ruhanen

Työn nimi / Arbetets titel – Title

Inferences of magma interaction processes from mineral chemistry and geothermobarometry of mingled and mixed rock types in the Ahvenisto complex, SE Finland

Oppiaine /Läroämne – Subject

Geology

Työn laji/Arbetets art – Level	Aika/Datum – Month and year	Sivumäärä/ Sidoantal – Number of pages
Master´s thesis	05/2022	47 + 6 appendices

Tiivistelmä/Referat – Abstract

The 1.64 Ga Ahvenisto complex in the southeastern Finland, is an anorthosite-mangerite-charnokite-granite (AMCG) suite, which has been discovered to host conspicuous magma interaction structures formed in magma mixing and mingling. These structures form areas where the consequences of mingling are found as monzodioritic pillows and granitic veins forming net-veined complexes. Mixing of monzodioritic and hornblende granitic magmas has produced hybrid rocks with intermediate composition.

The main goals of the study were to report the major element mineral chemistry of the main minerals (plagioclase, alkali-feldspar, amphibole, and pyroxene) from the hybrid rocks, hornblende granite, and monzodiorite and to test the suitability of geothermobarometric methods for the rock types related to the different magma interaction structures and to evaluate crystallization pressures and temperatures of the pertinent magmas.

The magma interaction structures of the Ahvenisto complex are recognized in the mineral chemistry of the mingling and mixing related rocks. The mineral chemistry confirms that the hornblende-granite represents the most primitive granitic phase in the mixing set and the composition of the minerals change as the mixing proceeds towards the final hybrid rock. The mineral chemistry from the monzodiorites reveals that the monzodiorites from different areas of the Ahvenisto complex have distinguished features and they can be separated by their composition.

Hornblende-plagioclase thermobarometers and two-pyroxene thermometers were used, and the results were compared to the previous studies related to the emplacement conditions of the Ahvenisto complex. The hornblende-plagioclase thermobarometers suggest that the crystallization of the mixing related rocks took place at ~790–860°C. For the temperature results, pressures of 100 MPa and 300 MPa were used based on earlier studies and a conclusion is drawn that the pressure has had only minor impact on the temperature. The two-pyroxene thermometers show similar regional difference for the crystallization temperatures of the monzodioritic rocks as recognized in the mineral chemistry. The results from the two-pyroxene thermometers show wider variation in the temperatures, which leaves some uncertainty on the liability of the results. The variation is mainly explained by the mineral chemistry of the mafic silicate minerals in the Ahvenisto complex rocks being very iron-rich and outside the calibration standards of the geothermobarometers.

Avainsanat – Nyckelord – Keywords

Geothermobarometry, hornblende-plagioclase thermobarometry, two-pyroxene thermometry, mineral chemistry, mingling, mixing, viscosity, Ahvenisto complex

Säilytyspaikka – Förvaringställe – Where deposited

HELDA – University of Helsinki Digital Repository

Muita tietoja – Övriga uppgifter – Additional information

HELSINGIN YLIOPISTO
HELSINGFORS UNIVERSITET
UNIVERSITY OF HELSINKI

Tiedekunta/Osasto Fakultet/Sektion – Faculty	Laitos/Institution– Department
Matemaattis-luonnontieteellinen tiedekunta	Geotieteiden ja maantieteen laitos

Tekijä/Författare – Author

Hanna-Kaisa Ruhanen

Työn nimi / Arbetets titel – Title

Inferences of magma interaction processes from mineral chemistry and geothermobarometry of mingled and mixed rock types in the Ahvenisto complex, SE Finland

Oppiaine /Läroämne – Subject

Geologia (petrologia ja taloudellinen geologia)

Työn laji/Arbetets art – Level	Aika/Datum – Month and year	Sivumäärä/ Sidoantal – Number of pages
Pro Gradu	05/2022	47 + 6 liitettä

Tiivistelmä/Referat – Abstract

1.64 Ga Ahveniston anortosiitti-mangeriitti-charnokiitti-graniitti (AMCG) -kompleksi sijaitsee Kaakkois-Suomessa. Aiemmissa tutkimuksissa alueelta on havaittu löytyvän magman vuorovaikutusrakenteita, jotka ovat syntyneet magman sekoittumisen ja sekaantumisen myötä. Nämä rakenteet muodostavat alueita, joissa sekoittuminen esiintyy monzodioriittisten tyynyjen ja graniittisten juonien synnyttäminä verkko-juoni (net-veined) komplekseina. Monzodioriittiset ja graniittiset magmat ovat sekoittuessaan muodostaneet koostumukseltaan keskiasteisia hybridikiviä.

Tutkimuksen tavoitteena oli raportoida monzodioriittisten kivien, sarvivälkegraniitin ja hybridikivien pääminerаalien (plagioklaasi, kalimaasälpä, amfiboli, pyrokseeni) pääalkuaineiden mineraalikoostumus sekä testata geotermobarometrien soveltumista magman eri vuorovaikutusrakenteisiin liittyvien kivityyppien kiteytymispaineiden ja -lämpötilojen arvioimiseen.

Ahveniston kompleksin magman vuorovaikutusrakenteet voidaan tunnistaa magman sekoittumiseen ja sekkantumiseen liittyvien kivityyppien mineraalikemiassa. Mineraalikemia vahvistaa, että sarvivälkegraniitti on sekoittumissarjan primitiivisin graniittifaasi ja, että sen mineraalikoostumus kehittyy sekoittumisen myötä siirryttäessä sarjassa kohti lopullista hybridikiveä. Monzodioriittien mineraalikemia paljastaa, että Ahveniston monzodioriittisten kivien mineraalikoostumuksessa on alueellisia eroja, joiden perusteella ne voidaan tunnistaa.

Sarvivälke-plagioklaasi termobarometrejä ja kahden pyrokseenin termometrejä käytettiin Ahveniston kompleksin paikalleen asettumisen olosuhteiden selvittämiseen ja tuloksia verrattiin aiempiin tutkimuksiin. Sarvivälke-plagioklaasi termobarometrit ehdottivat sekoittumisrakenteisiin liittyvien kivien kiteytymislämpötilaksi ~790–860°C. Lähdeaineiston perusteella todennäköisiksi paineolosuhteiksi valittiin 100 MPa ja 300 MPa. Tulosten perusteella voidaan kuitenkin päätellä, että paineella on ollut vain vähäinen vaikutus kiteytymislämpötiloihin. Kahden pyrokseenin termometrien perusteella voidaan monzodioriittisissä kivissä erotella samankaltainen alueellinen ero myös kiteytymislämpötilojen suhteen, kuten mineraalikoostumuksen suhteen. Kahden pyrokseenin thermometrien lämpötilatuloksissa esiintyy jonkin verran vaihtelua, joka aiheuttaa epävarmuutta tulosten tulkinnassa, Vaihtelu selittyy sillä, että termometrien kalibrointistandardit eivät kata Ahveniston kompleksin mafisten silikaattimineraalien kaltaista, erittäin korkean Fe/Mg suhteen omaavaa mineraaliparageneesiä.

Avainsanat – Nyckelord – Keywords

Geotermobarometria, sarvivälke-plagioklaasi termobarometri, kahden pyrokseenin termometri, mineraalikemia, sekaantuminen, sekoittuminen, viskositeetti, Ahveniston kompleksi

Säilytyspaikka – Förvaringställe – Where deposited

HELDA – Helsingin yliopiston digitaalinen arkisto

Muita tietoja – Övriga uppgifter – Additional information

CONTENTS

1. INTRODUCTION

Proterozoic anorthosite-mangerite-charnokite-granite (AMCG) associations are an important example of bimodal (felsic-mafic) magmatism (e.g., Emslie 1978, Emslie et al. 1994). Anorthositic rocks represent the mafic members of these suites and are usually associated with felsic mangerite-charnokite-granite rocks. AMCG complexes are found in almost all continents, and classical localities are, for example Grenville and Labrador in Canada (e.g., Emslie 1978, Heinonen et al. 2015).

The Ahvenisto complex in southeastern Finland is an AMCG suite that hosts prominent examples of bimodal magmatism related to rapakivi granites (Alviola et al. 1999, Rämö and Haapala 2005). It is related to the Wiborg batholith, which is the largest (~19 000 km^2) rapakivi intrusion in Finland (Rämö and Haapala 2005). The bimodal magmatism is evident in magma interaction structures of mixing and mingling, which can be observed in the Ahvenisto complex. Same kind of structures are present also in other locations in Finland e.g., Jaala-Iitti (Salonsaari 1995, Elliott 2001) and Åland (Bergman 1986, Eklund 1991). In the recent years, the Ahvenisto complex has become a key location in petrogenetic studies of AMCG suites in the Fennoscandian shield area (Alviola et al. 1999, Rämö and Haapala 2005, Heinonen 2012, Fred et al. 2019, 2020, Heinonen et al. 2020).

1.1. Magma interaction structures

In the evolution of rocks in AMCG suites, bimodal (felsic-mafic) magmatism occurs when partial melting of crustal material forms silicic magmas due to the heat derived from uprising and crystallizing mantle-derived basic magmas (Emslie 1978). These events affect the thermal, isotopic, and chemical evolution of the silicic magmas (Wiebe 1996). Magma interaction structures resulting from different interaction processes (e.g., mixing and mingling), are visible evidence of simultaneous occurrence of two or more magmas with contrasting (silicic-basic) compositions (Marshall and Sparks 1984).

End-member magmas with contrasting composition but similar physical properties can completely chemically mix to form a homogenous new magma that crystallizes to form

a hybrid rock with composition between the end-member magmas mixed (Marshall and Sparks 1984). Hybrid rocks can form, when both magmas are in near-liquid conditions at the same temperature and the relative amount of the basic magma (in basaltic compositions) is at least 50 %, for it to be able to chemically mix with a silicic magma (Sparks and Marshall 1986). According to Walker and Skelhorn (1966), the recognition of the silicic end-member of a hybrid rock can be studied by examining xenocrysts of minerals in the hybrid present as phenocrysts in the silicic end-member. If the xenocrysts have similar composition as the phenocrysts, they provide strong evidence that the silicic end-member was involved in the genesis of the hybrid rock.

When the end-member magmas have too contrasting physical properties and compositions, they are not able to chemically mix, and instead commingling takes place (Marshall and Sparks 1984). The end-members remain as their own heterogenous phases and form mingling structures, such as fingers, pipes, pillow structures, and net-veined complexes (Walker and Skelhorn 1966). Mingling structures usually show evidence of chemical and/or thermal exchange at the margins of the silicic and basic components. Observed features can be, for example flame features, chilled margins, or margins with finer grain size. (e.g., Walker and Skelhorn 1966, Marhall and Sparks 1984, Wiebe 1996).

1.2. Principles of mineralogical geothermobarometry

In the latter half of the 20th century mineralogical geothermobarometry and its applications have established their role as an important tool in geological, mineralogical, and petrological research (Anderson et al. 2008). The estimation of pressure (P) and temperature (T) are important in the study of evolution and intrusion mechanisms of magmas. There are tens of individual methods developed for mineralogical geothermobarometry and researchers are constantly looking for new ones (Putirka 2008).

According to Putirka (2008), when a geothermobarometer is developed, the main goal is to find mineral reactions whose chemical equilibrium imposes significant differences in either the entropy (ΔS) or the volume (ΔV) of the reactants and the products. When the difference is large for entropy, the reaction is suitable for geothermometry, and when the

difference is large for volume, the reaction is suitable for geobarometry. Some reactions can even be suitable for both.

After Putirka (2008), the single most important equation in geothermobarometry is the basic thermodynamic equation:

$$-RTlnKeq = \Delta Gr° \qquad (1)$$

where R is the gas constant (R = 1.9872 cal/K·mole, or 8.3144 J/dK·mole), ΔGr° is the Gibbs free energy change for standard state, and K_{eq} is the equilibrium constant of the reaction. Differences in ΔS and ΔV can cause K_{eq} to vary as function of pressure (P) and/or temperature (T). The basis for any geothermobarometer, is a thermodynamic model, where K_{eq} can be quantitatively compared in relation to P and/or T.

1.2.1. Hornblende-plagioclase thermobarometry

Blundy and Holland (1990) first developed the hornblende-plagioclase thermometer (hereafter referred to as thermometer A) for geothermometry of calc-alkaline igneous rocks. Holland and Blundy (1994) further introduced some calibrations and developed the revised hornblende-plagioclase thermometer (hereafter referred to as thermometer B). Both thermometers (A and B) were generated by using total aluminum content in amphiboles (hornblende) coexisting in equilibrium with plagioclase and they are based on the Ca and Na equilibrium exchange between these minerals.

According to Holland and Blundy (1994), thermometer A is based on the reaction between edenite and tremolite and thermometer B is based on the reaction between edenite and richterite. Thermometer A is applicable with assemblages that include quartz (silica-saturated rocks), but thermometer B can also be used on assemblages without quartz (silica-undersaturated rocks). These thermometers have been calibrated with a wide compositional range of synthetic and natural amphiboles and they take into account the non-ideal mixing of the minerals as well.

The restrictions for the use of hornblende-plagioclase thermometers are:

A) Temperature in the range of 400–900 °C, amphibole that have Na>0.02 pfu, Al^{VI}<l.8 pfu, and Si in the range of 6.0–7.7 pfu, and plagioclase with X_{An}<0.90 (Holland and Blundy 1994).
B) Temperature in the range of 500–900 °C, plagioclase with X_{An} = 0.1–0.9, amphibole with Na^{M4}>0.03 pfu, Al^{VI}<1.8 pfu, and Si in the range of 6.0–7.7 pfu (Holland and Blundy 1994).

1.2.2. Two-pyroxene thermometry

Several applications for two-pyroxene thermometry have been developed since the 1970s (e.g., Wood and Banno 1973, Wells 1977, Lindsley and Andersen 1983, Mercier et al. 1984). Two-pyroxene thermometers are based on coexisting high-Ca and low-Ca pyroxenes and the diopside-enstatite miscibility gap (Wells 1997). As the Ca content of high-Ca pyroxene (augite) decreases with increasing temperature, at the same time the Ca content of low-Ca pyroxene (orthopyroxene or pigeonite) increases (Lindsley and Andersen 1983). During the calibration of the thermometers, the equilibrium of the system is tested with the distribution of Mg and Fe between pyroxenes (Putirka 2008).

According to Lindsley (1983), the two-pyroxene thermometer is applicable for a broad variety of igneous and metamorphic rocks containing naturally coexisting pyroxenes. Restrictions for the use of a thermometer are: Wo+En+Fs > 90%, pressure (P) 0.1–1500 MPa, temperature (T) 800–1200 °C, and the pyroxenes should not show evidence of granule exsolution. In spite of many inaccuracies reported (e.g., Wells 1977, Lindsley and Andersen 1983) regarding these thermometers, most of the experimental data can be fitted to a linear relation between lnK and l/T using the ideal two-site mixing model by Wood and Banno (1973) for the diopside-enstatite miscibility gap.

1.3. Objectives of this study

Crystallization conditions of the ubiquitous magma interaction structures (pillow and net-veined structures caused by to magma mingling and hybrid rocks generated by magma mixing) and related rock types in the Ahvenisto complex are not very well known (cf.

Fred et al. 2019). Better knowledge of the genetic circumstances of these would provide valuable information about the emplacement history of the Ahvenisto complex and shed light into the emplacement history of the entire Wiborg magma system in general. The main objective of this thesis is to continue the study of rock types related to the magma interaction structures in the Ahvenisto complex launched in 2015 (Fred 2017; see also Fred et al. 2019, 2020).

In order to successfully examine the evolution of hybrid rocks, it would be important to determine the origin of the alkali-feldspar phenocrysts observed in them (Walker and Skelhorn 1966). It is also important to analyze minerals such as amphibole and biotite, which crystallized after the chemical mixing had taken place (Salonsaari 1995). The best way to study this, is to examine the mineral chemistry of the assumed mafic and felsic end-members involved in mixing and the produced hybrid rocks. The results could be used to refine the mixing and mingling hypotheses developed by Fred (2017; see also Fred et al. 2019) for the Ahvenisto complex rocks.

The focus of this study is to report the chemical composition of the main minerals (plagioclase, alkali-feldspar, amphibole, pyroxene) from the hybrid rocks, hornblende granites, and monzodiorites involved in the magma interaction processes in the Ahvenisto complex and to test the suitability of geothermobarometric methods to evaluate crystallization pressures and temperatures of the pertinent magmas. The aim is to find out: 1) if the crystallization temperatures and pressures can reliably be defined by using plagioclase-amphibole and two-pyroxene geothermobarometers, 2) to study the relationships of the mineral phases common to the related rock types, and 3) to search evidence for the intrusion mechanics. The results of this study provide new data, which can be compared with data acquired in previous studies (e.g., Salonsaari 1995, Elliott 2001, Kivisaari 2015, Fred 2017, Fred et al. 2019, 2020, Heinonen et al. 2020) from the Wiborg rapakivi granite suite.

2. GEOLOGICAL BACKGROUND

2.1. The Ahvenisto complex

The ~1640 Ma (Alviola et al. 1999, Heinonen et al. 2010b) Ahvenisto complex is one of the smaller intrusive bodies, which are related to the Paleoproterozoic anorogenic magmatism in the Wiborg batholith area in southeastern Finland (Fig. 1). The other two are the Suomenniemi (Rämö 1991) and the Jaala-Iitti complexes (Salonsaari 1995, Elliott 2000). The Ahvenisto complex is located northwest of the main Wiborg batholith and consists of a granitic intrusion surrounded by a mafic arc consisting of leucogabbronorite, leuconorite, leucotroctolite, and anorthosite, and a monzodioritic ring-dyke system (e.g., Rämö and Haapala 2005, Heinonen et al. 2010b). In addition to the rapakivi occurrences in southeastern Finland, there are several other localities with rapakivi granites also in southwestern Finland (Rämö and Haapala 1995) e.g., Laitila (Vorma 1976), Vehmaa (Kanerva 1928), and Åland (Bergman 1986, Eklund 1991).

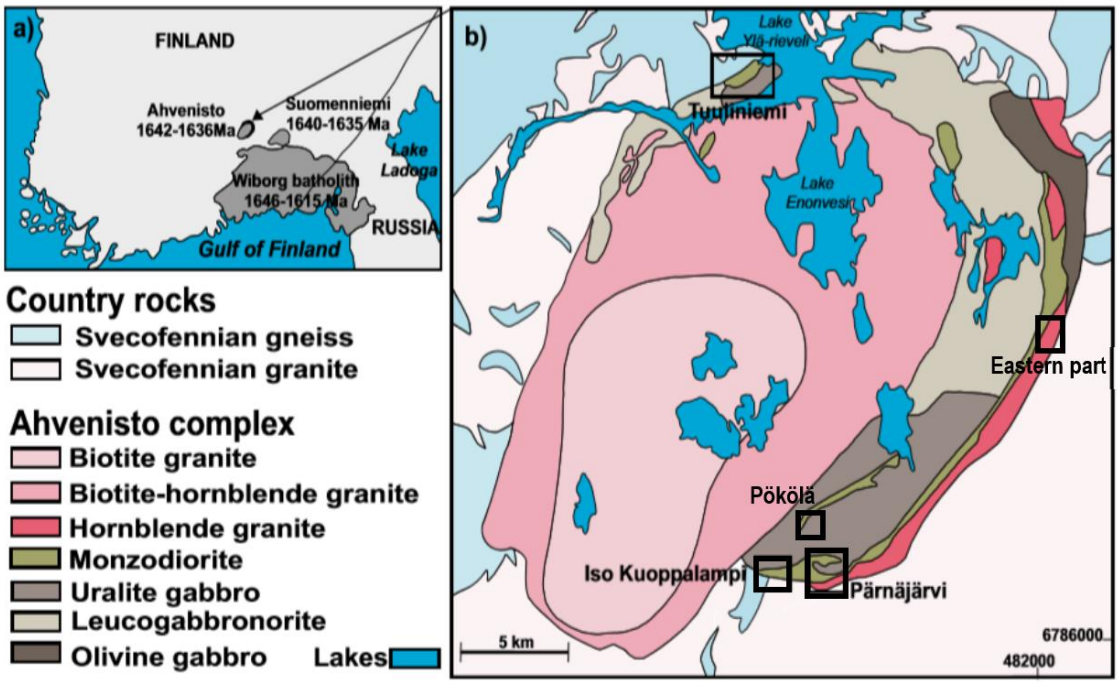

Figure 1. a) The location of the Ahvenisto complex in southern Finland relative to the main Wiborg batholith and b) a simplified lithological map of the Ahvenisto complex and the locations of the study areas (modified from Fred et al. 2019).

At the current erosional level, the Ahvenisto complex covers an area of ca. 350 km² of which granitic rocks cover ca. 70% and gabbro-anorthositic rocks 25% (Alviola et al. 1999). Monzodioritic rocks with mafic to intermediate compositions are found only as a minor (<5%) component (Alviola et al. 1999, Fred et al. 2019). At the current level of exposure of the Fennoscandian shield, the Ahvenisto complex hosts the most significant localities of massif-type anorthosites and associated monzodioritic rocks (Rämö and Haapala 2005). Other known locations of monzodioritic rocks related to rapakivi granites in Finland are in Åland (Eklund 1991).

According to U-Pb dating (Alviola et al. 1999, Heinonen et al. 2010b), the Ahvenisto complex was emplaced at 1644 to 1629 Ma and all of the dated rock types show overlapping ages within analytical errors. The complex intruded the Paleoproterozoic (ca.1.93–1.80 Ga) Svecofennian country rocks and the contact between the complex and the surrounding metamorphic rocks is usually sharp (Alviola et al. 1999) locally, however, very complex contact zones are also observed (Fred et al. 2019). Field studies (Johanson 1984, Alviola et al. 1999, Heinonen et al. 2010b) suggest that the granitic rocks are the youngest and cut the anorthositic and monzodioritic rocks. The monzodioritic rocks are the youngest of the mafic rocks and crosscut the anorthositic rocks. However, evidence of simultaneous emplacement of the earliest silicic and last basic magmas are observed as interaction structures between the hornblende granites and monzodioritic rocks of the complex (e.g., Alviola et al. 1999, Fred et al, 2019).

Isotopic evidence (Heinonen et al. 2010a, 2010b, 2015, Heinonen 2012) supports the hypothesis that the parental magmas of the felsic (rapakivi granites) and mafic (anorthositic and monzodioritic) rocks had separate sources. The mafic rocks show isotopic signature of a depleted mantle source with significant crustal contamination, whereas the felsic rocks show isotopic signature of crustal origin with a minor mantle component.

2.2. Magma interaction structures in the Ahvenisto complex

The Ahvenisto complex has been discovered to host conspicuous magma interaction structures due to magma mixing and mingling (e.g., Savolahti 1956, Johanson 1984,

Alviola et al. 1999, Fred et al. 2019). These structures are result of the bimodal magmatism with different simultaneous interaction states of the mafic and felsic magmas (e.g., Alviola et al. 1999, Heinonen et al. 2010b; see also Marshall and Sparks 1984). Similar interaction between felsic and mafic magma has also been studied from other localities related to rapakivi granite magmatism in Finland, for example in Åland (Lindberg and Eklund 1988, Eklund et al. 1993).

Detailed mapping of the magma interaction structures in the Ahvenisto complex was conducted by Fred (2017; see also Fred et al. 2019) and examples of the related rock types are presented in Figure 2. Recent fieldwork conducted in the area (Fred et al. 2019, 2020) has revealed that the mingling and mixing structures are much more common than previously thought. Mingling structures are observed trough-out the monzodioritic dikes and hybrid rocks in several locations in the southeastern parts of the complex. Evidence of magma mixing is observed between monzodioritic and hornblende granitic magmas as formation of a new hybrid magma (Fred et al. 2019), which formed rocks with intermediate compositions with alkali-feldspar phenocrysts in a relatively basic groundmass (Fig. 2b; Johanson 1984, Rämö 1991, Alviola et al. 1999, Fred et al. 2019).

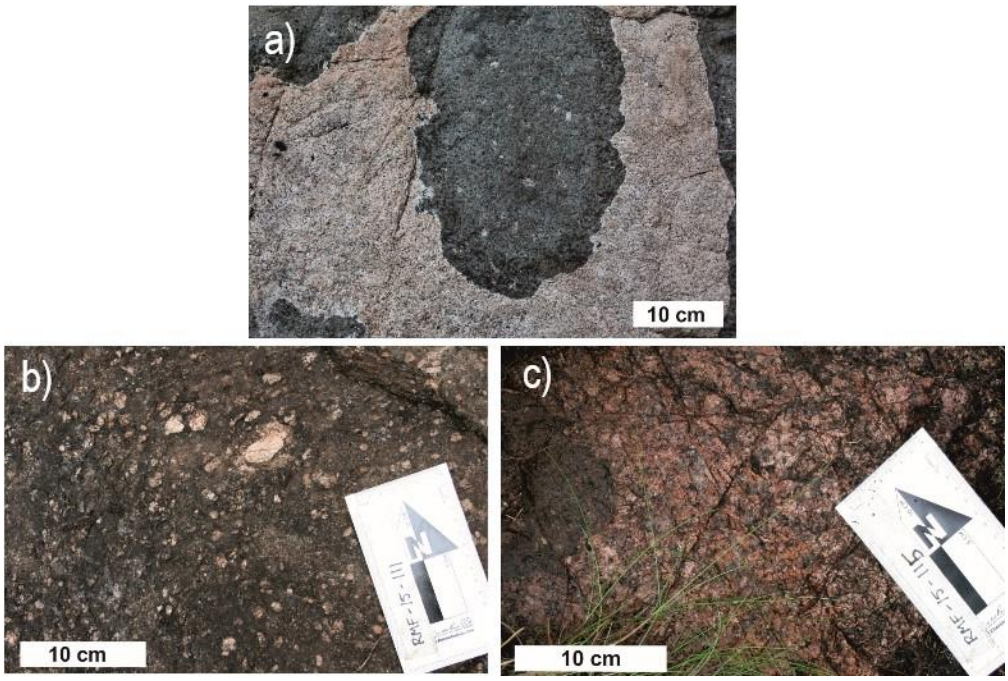

Figure 2. Examples of rock types related to the magma interaction processes in the Ahvenisto complex: a) monzodioritic pillows and net-veined granitic rocks, b) hybrid rocks, and c) hornblende granites (modified from Fred et al. 2019, photos Aku Heinonen).

Evidence of mingling processes between monzodioritic and granitic magmas is observed as monzodioritic pillows and net-veined granitic rocks (Fig. 2a; Alviola et al. 1999, Fred et al. 2019).

2.3. Geochemical and viscosity modeling of the interaction structures in the Ahvenisto complex

Fred et al. (2019) studied the geochemistry and petrography of the magma interaction structures and related rock types in the Ahvenisto complex. Three geochemically and mineralogically deviant monzodioritic groups were identified: olivine monzodiorites, pillow-structured monzodiorites, and massive monzodiorites (Fred et al. 2019). To study the different interaction scenarios between the magmas that crystallized the monzodioritic rocks and concomitant granitic magmas, geochemical and viscosity modeling were conducted. The mixing scenario was studied by chemical mixing of the hornblende granite with different monzodioritic compositions (massive monzodiorite, pillow-structured monzodiorite, and olivine monzodiorite) and comparing the calculated mixing trends to the observed hybrid rock compositions.

In the geochemical mixing models, the massive quartz monzodiorite was found to be the most probable mafic end-member, and the hornblende granite to represent the felsic end-member (Fig. 3; Fred et al. 2019). In addition, field evidence suggests that the most primitive olivine monzodiorite did not interact with the felsic magma but only contained some smaller inclusions of the granitic material. The monzodioritic magma (i.e. pillow-structured monzodiorites) with the composition between the most evolved (massive monzodiorites) and most primitive monzodiorites (olivine monzodiorites) formed the mingling structures together with the felsic magma.

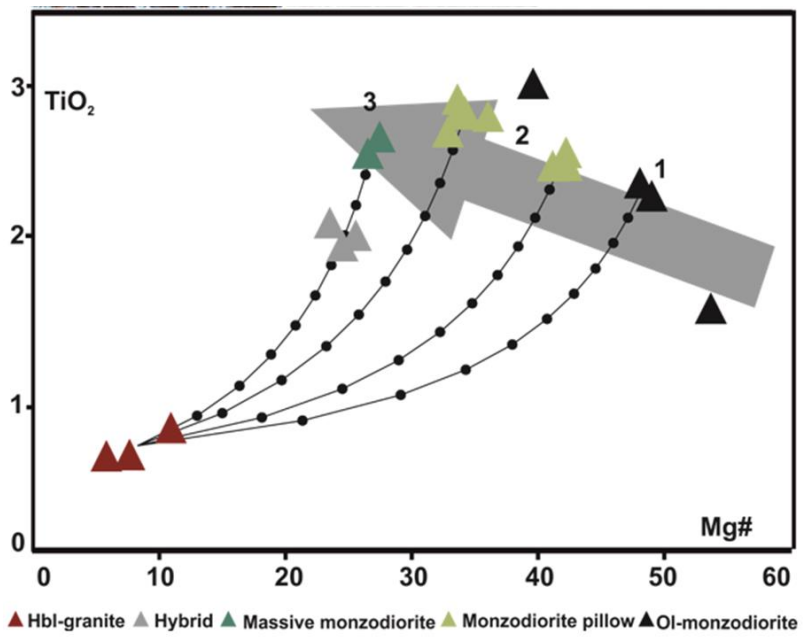

Figure 3. Mixing scenario between hornblende granite and monzodioritic rocks with different chemical compositions: 1) olivine mozodiorite, 2) monzodiorite pillow, and 3) massive monzodiorite on a Mg# vs. TiO_2 (wt-%) diagram. Grey arrow represents the possible fractionation trend of the monzodioritic rocks (modified from Fred et al. 2019).

Viscosity (log η) and temperature (T) play an important role in the generation of magma interaction structures and in a classic situation, the silicic magma has higher log η and lower T than the basic magma (Sparks and Marshall 1986). The viscosity calculations by Fred (2017), indicate however, that at near-liquidus temperatures, the relative viscosities can be even opposite in these rocks, resulting in different kinds of magma interaction structures. The presumption is that a considerable amount of heat can be transferred from a large quantity of basic magma to the silicic magma to lower its viscosity. As the mafic magma cools down and crystallizes at the same time, it gets more viscous, and the viscosity difference of the magmas decreases and can even be reversed (Sparks and Marshall 1986).

From the results of the melt viscosity modeling, Fred (2017) concluded that the mingling of monzodioritic and granitic magmas (Fig. 4a) occurred when the granitic magma was less viscous and mingled between the pillows formed by the more viscous monzodioritic magma. The mixing of monzodioritic and granitic magmas (Fig. 4b) took place in conditions where both magmas were simultaneously in near-liquid conditions and had

similar viscosities and temperatures. The interaction occurred at an intermediate stage in the magmatic evolution of the Ahvenisto complex, when the first fractions of silicic (granitic) magmas and last fractions of basic (monzodioritic) magmas were at near-liquid conditions at the same time.

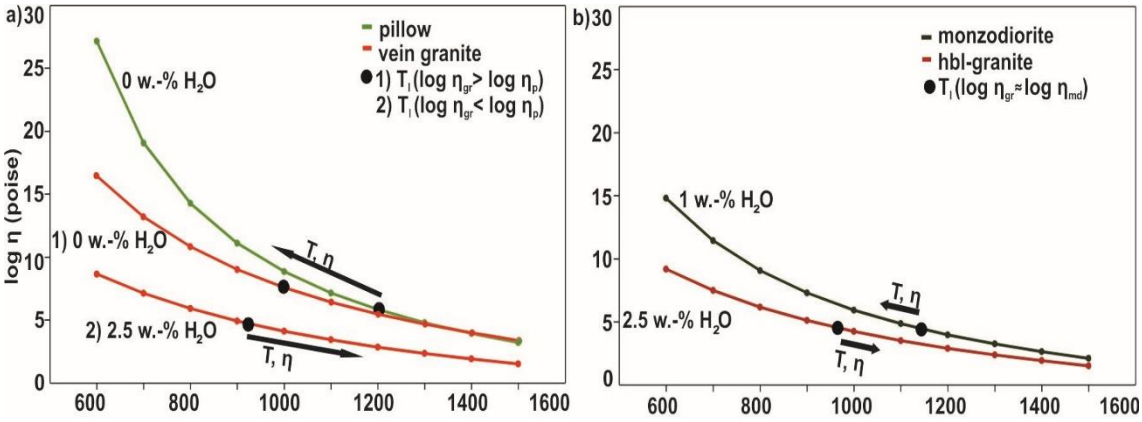

Figure 4. Melt viscosity models for a) monzodioritic pillows and granitic veins and b) massive monzodiorite and hornblende granite, gr=granite, md=monzodiorite, and p=pillow (modified from Fred 2017).

3. METHODS AND MATERIAL

3.1. Material from previous studies

The samples used in this study were collected from the Ahvenisto complex area by R. Fred and A. Heinonen during 2014, 2015, and 2018. Most of the samples were previously used in a MSc thesis project conducted by Fred (2017) and in subsequent studies (Fred et al. 2019, 2020). The samples were collected, with a hammer or a rock saw, from five different study areas (Fig. 1): Tuuliniemi, Iso Kuoppalampi, Pökölä, Pärnäjärvi, and the eastern part of the Ahvenisto complex. Detailed coordinates of the sample locations are listed in Appendix 1.

In addition to the data produced in this study, whole-rock major and trace element geochemical XRF (X-ray fluorescence) and ICP-MS (inductively coupled plasma mass spectrometry) data (Fred 2017, Fred et al.2020), and supplementary mineral chemical EMPA data (Fred et al. 2020) related to an ongoing PhD thesis project are also available for this and possible future studies.

3.2. Samples and sample preparation

The thin sections were prepared, and the petrography of the samples was carefully studied with a polarization microscope (Nikon LABPHOT2-POL) at the Department of Geosciences and Geography, University of Helsinki. The close-up photomicrographs were taken of the main minerals (plagioclase, alkali-feldspar, amphiboles, biotite clinopyroxene, and orthopyroxene) to be analyzed by EMPA (electron microprobe analyzer). The photomicrographs were taken with Leica DF C450 camera mounted on a Leica DM 2500P polarization microscope using LAS V4.4 software. The thin sections selected for EMPA analysis were also photographed with a DSLR (digital single-lens reflex) camera (Canon 6D with a 100 mm F/2.8 L macro-objective). The thin sections were cleaned, and carbon coated prior to EMPA analysis.

EMPA analyses were conducted from nine thin sections in total, grouped in three different sets (Table 1): mingling set, mixing set, and monzodiorite set. Seven (marked with * in Table 1) of the nine thin sections have been used also in previous studies (Fred et al. 2019), but thin sections RMF-18-077-A and RMF-18-188-A, are studied for the first time in this study. The samples were collected carefully so that they best represent the different types of magma interaction structures in the Ahvenisto complex. Distinct locations of rocks with mingling structures and hybrid rocks were chosen and the samples were collected from separate parts of these rocks for possible evaluation of chemical and mineralogical differences. The samples of the “mixing set” and “mingling set” are from the Pärnäjärvi area. The samples of the “mixing set” consist of hornblende granite, hybrid rock, and the contact between these rock types. In the “mingling set”, the samples are from the center of a monzodioritic pillow, the center of a leucocratic vein granite, and from the contact between the same pillow and vein (Fred et al. 2019). The samples of the “monzodiorite set” were selected from different parts of the Ahvenisto complex; the eastern part, Pökölä area, and Pärnäjärvi area to compare their mineralogical and mineral chemical characteristics.

Table 1. Thin section sets for microprobe analysis including rock type, name of the set and analysed minerals.

Sample ID	Rock type	Set	Mineral
RMF-15-115-A.H1 (*)	Contact of hornblende granite and hybrid rock	Mixing	hbl, pl, kfs
RMF-15-115-B.H1 (*)	Hornblende granite	Mixing	hbl, pl, kfs
RMF-15-115-C.H1 (*)	Hybrid rock	Mixing	hbl, pl, bi
APHE-14-011.5.H1 (*)	Contact of monzodioritic pillow and vein granite	Mingling	pl, bi
APHE-14-011.5.H3 (*)	Leucocratic vein granite	Mingling	pl, bi
APHE-14-011.E.H1 (*)	Monzodioritic pillow	Mingling	pl, bi
RMF-15-116-A.H1 (*)	Monzodiorite	Monzodiorite	opx, cpx, pl
RMF-18-077-A	Monzodiorite	Monzodiorite	opx, cpx, pl
RMF-18-188-A	Monzodiorite	Monzodiorite	opx, cpx, pl

Mineral abbreviations: hbl = hornblende, pl = plagioclase, kfs = alkali-feldspar, bi = biotite, opx = orthopyroxene, cpx = clinopyroxene
* = used in Fred et al. (2019)

3.3. Analytical methods

Major element mineral chemical compositions were analyzed with Cameca SX100 electron micro-probe analyzer (EMPA) in the Laboratory of Mineral Processing and Materials Research of the Geological Survey of Finland. The matrix correction was performed with PAP based online software (Pouchou and Pichoir 1986). The acceleration voltage, sample current, and beam diameter for the analyses were 15 kV, 20 nA, and ca. 5 μm, respectively. Major element mineral chemistry of the main minerals was

determined as quantitative mineral analysis with wavelength-dispersive spectroscopy (WDS).

From the mingling-set plagioclase and biotite, from the mixing set hornblende, plagioclase, alkali feldspar, and biotite, and from the monzodiorite set orthopyroxene, clinopyroxene, and plagioclase were analyzed. In total, seventeen elements (Si, Ti, Al, Cr, V, Fe, Mn, Mg, Ca, Na, K, Sr, Ba, Ni, S, Zn and P) were measured from all minerals. The results of the electron microprobe analyses are presented in Appendices 2a–2e.

The standards (Astimex Standards Ltd, Toronto) used in the analysis for different elements were: Si K_a diopside, Mg K_a diopside, Ca K_a diopside, Fe K_a almandine, Al K_a almandine, Na K_a tugtupite, Cl K_a tugtupite, Sr L_a celestine, P K_a apatite, Mn K_a rhodonite, Ti K_a rutile, Cr K_a ^{53}Cr chromite, Zn K_a sphalerite, Ni K_a pentlandite, S K_a pentlandite, F fluorite, K K_a sanidine, and Ba L_a barite. The standard deviation for the measurements is <1%.

4. RESULTS

4.1 Petrography

Nine new thin sections were prepared for this study by laboratory engineer R. Michallik at the Department of Geosciences and Geography, University of Helsinki. The samples (Table 2) are from (Fig.1) Tuuliniemi, Pökölä, Iso Kuoppalampi, and the eastern part of the complex. Six of the samples are from massive monzodiorites, one is from a hornblende granite, and two are from pillow monzodiorites from the mingling structures.

Table 2. New thin section samples.

Sample ID	Rock type	Study area
RMF-18-007-A	Hornblende granite	Tuuliniemi
RMF-18-013-A	Monzodiorite	Tuuliniemi
RMF-18-077-A	Monzodiorite	Pökölä
RMF-18-078-A	Monzodiorite	Pökölä
RMF-18-110-A	Monzodiorite pillow	Iso Kuoppalampi
RMF-18-118-C	Monzodiorite	Iso Kuoppalampi
RMF-18-252-A	Monzodiorite pillow	Iso Kuoppalampi
RMF-18-168-A	Monzodiorite	Eastern part
RMF-18-188-A	Monzodiorite	Eastern part

In general, plagioclase seems to form about 30 vol% of the monzodioritic rocks. Albite and Carlsbad twinning are quite common and in some of the samples, plagioclase forms glomeroporphyritic textures. According to the IUGS classification of the plutonic igneous rocks (Le Bas and Streckeisen 1991), for monzodiorite, plagioclase compositions should be $An_{<50\%}$. The petrographic studies suggest that the composition of the plagioclase in these rocks would correspond to andesine ($An_{30–50\%}$).

In addition to plagioclase, other main minerals in the different monzodioritic rocks are amphibole, biotite, pyroxene, chlorite, and alkali feldspar. Chlorite seems to be an alteration product of biotite. Hornblende has typical diamond-shaped [110]-type cleavage and dark green to brown pleochroism. Thin opaque lamellae are common in pyroxenes and orthopyroxene exsolution lamellae in clinopyroxene and vice versa are also common.

Most common accessory minerals are quartz, apatite, zircon, and opaque minerals. Quartz normally appears as anhedral grains with undulatory extinction. Acicular apatite is very commonly overprinting other minerals. Zircon is found in some of the samples as euhedral grains. The opaque minerals are in general rounded, or teardrop-shaped, but in some of the samples, also acicular forms are observed.

4.1.1. Tuuliniemi

From Tuuliniemi area there are two samples: RMF-18-007-A represents the hornblende granite and RMF-18-013-A massive monzodiorite. The minerals in the hornblende granite are equigranular and mainly subhedral to anhedral. Main minerals are plagioclase, hornblende, alkali feldspar, biotite, and quartz. All minerals, except biotite show alteration and biotite is the only euhedral mineral. The alteration is visible, for example, as sericite and myrmekite in the feldspars. The amount of plagioclase (~30 vol%) is higher than the amount of alkali feldspar (~15 vol%). Hornblende is the main mafic phase (~25 vol%) and it is usually poikilitic. The amount of biotite is ~15 vol% and quartz ~10 vol%. Quartz has skeletal and anhedral appearance with undulatory extinction. The most notable accessory phases are apatite, zircon, and fluorite.

The massive monzodiorite is presented in Figure 5. Both pyroxenes are present in the groundmass, but orthopyroxene is more abundant (~35 vol%) compared to clinopyroxene (~10 vol%). Other minerals in the groundmass are plagioclase (~30 vol%), hornblende (~10 vol%), and alkali feldspar (~10 vol%). Accessory minerals are biotite, quartz, zircon, apatite, rutile, and opaque minerals. Minerals are mainly inequigranular and subhedral to anhedral as only zircon and apatite are euhedral. Hornblende is present also as poikilitic phenocrysts.

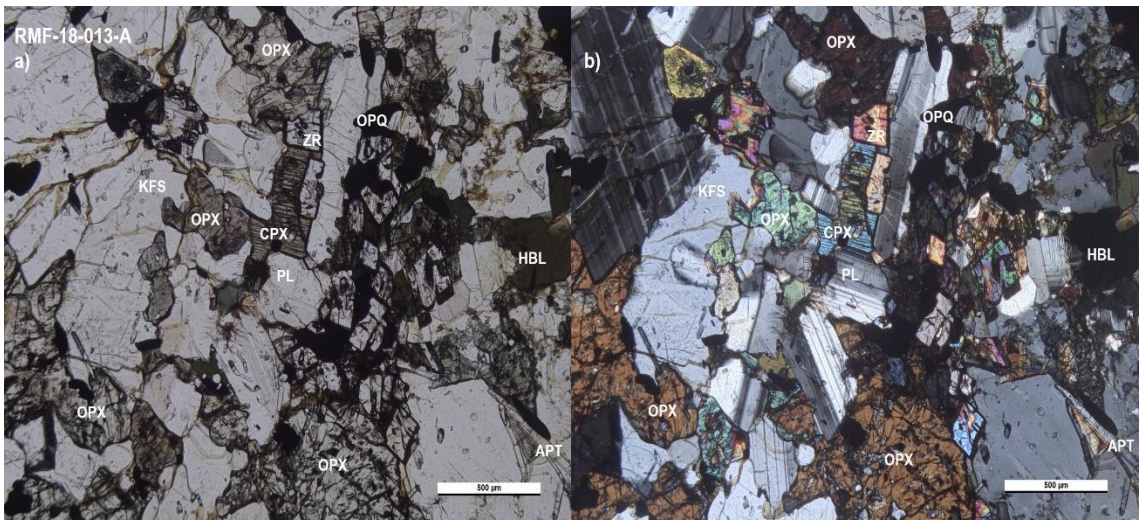

Figure 5. Photomicrograph of monzodiorite from Tuuliniemi (RMF-18-013-A) in a) plane-polarized and b) cross-polarized light, showing some petrographic observations of the sample: the higher amount of orthopyroxene (30 vol%) compared to clinopyroxene (~10 vol%) and coarser apatite crystals. The abbreviations are, cpx = clinopyroxene, opx = orthopyroxene pl = plagioclase, hbl = hornblende, kfs = alkali feldspar, apt = apatite, zr = zircon, and opq = opaque.

4.1.2. Pökölä

The two massive monzodiorite samples (RMF-18-077-A and -078-A) from Pökölä show evidence of alteration probably caused by magma mingling. Minerals are inequigranular and subhedral to anhedral. In the sample RMF-18-077-A, plagioclase (~30 vol%) is observed as subhedral phenocrysts (0.5 to 1.5 mm) and as part of the groundmass with fine grainsize. Both pyroxenes are present, orthopyroxene is more abundant (~25 vol%). The amount of clinopyroxene is ~10 vol%. Chlorite is one of the main phases (~8 vol%) in the groundmass and most likely represents alteration product of biotite. Biotite (~10 vol%) and hornblende (~5 vol%) appear as poikilitic phenocrysts. The grainsize of subhedral biotite is larger (up to 6 mm) compared to the finer grained groundmass. Because of the two completely different appearances of the biotite, it is likely that there are two generations of biotite present in this sample. Quartz is present only as minor phase as anhedral grains. Apatite, zircon, amphibole (most likely tremolite-actinolite), sericite, and opaque are other accessory minerals.

The other monzodiorite sample (RMF-18-078-A) is cut by a granitic dike. The dike consists of alkali feldspar, plagioclase, and quartz. The grain size of the vein is coarser compared to the monzodiorite. Close to the contact with the vein, the monzodiorite shows

stronger alteration: sericite in feldspars and chloritization of biotite. Otherwise, the monzodiorite shows similar features with the monzodioritic sample RMF-18-077-A.

4.1.3. Iso Kuoppalampi

Three samples from Iso Kuoppalampi area represent pillow monzodiorites (RMF-18-110-A and -252-A) and massive monzodiorite (RMF-18-118-C). In sample RMF-18-110-A, minerals show alteration, are inequigranular, mainly anhedral except for the plagioclase, which is subhedral. The main minerals are plagioclase (~30 vol%), biotite (~20 vol%), chlorite (~10 vol%), hornblende (10 vol%), amphibole (~10 vol%), and alkali feldspar (~10 vol%). The plagioclase phenocrysts (0.5 to 8 mm) form glomeroporphyritic textures and they contain small, needle-shaped exsolutions of sericite. The glomeroporphyritic plagioclase aggregates also commonly contain secondary amphibole and chlorite. The groundmass is fine-grained, and the appearance of the minerals is mossy. It consists mainly of feldspars, chlorite, and secondary, asbestiform amphibole pseudomorphs. This mineral with high interference colors is probably tremolite-actinolite. Some biotite and hornblende are present in the groundmass. Only few clinopyroxene relics with simple twinning are recognizable. Other accessory minerals are quartz, apatite, zircon, and opaque minerals.

Sample RMF-18-252-A is otherwise similar with the other pillow sample, but in addition to the pyroxene pseudomorphs it also contains some fresh pyroxenes. Also, there are some subhedral, healthy biotite phenocrysts. The main phase volumes are plagioclase (~30 vol%), biotite (~20 vol%), alkali feldspar (~15 vol%), chlorite (~15 vol%), clinopyroxene (~5 vol%), orthopyroxene (~5 vol%), and hornblende (~5 vol%).

Sample RMF-18-118-C represents a typical massive monzodiorite of the Ahvenisto complex with less alteration. Plagioclase (~30 vol%) is present in the fine-grained groundmass and as phenocrysts (up to 5 mm). The plagioclase phenocrysts are quite euhedral, slightly seritisized, and from glomerophorphyritic textures. The groundmass grains are skeletal. Anhedral poikilitic hornblende (~10 vol%) is also found as phenocrysts. Both pyroxenes are present in the groundmass. Clinopyroxene (~20 vol%) occurs with typical thin opaque lamellae and is slightly more abundant than

orthopyroxene (~15 vol%). The amount of alkali feldspar is ~15 vol% and biotite ~5 vol%. The accessory minerals are quartz, apatite, zircon, and opaque minerals.

4.1.4. Eastern part

Two massive monzodiorite samples from the Eastern part of the Ahvenisto complex were studied (RMF-18-168-A and -188-A). The groundmass grains are more equigranular and the grain size is generally smaller than (Figure 6), for example, in the monzodioritic sample (RMF-18-013-A) from Tuuliniemi. The minerals are also less altered and less skeletal. The plagioclase phenocrysts (1.5 to 5 mm) observed in massive monzodiorites from other areas in the Ahvenisto complex are missing from these samples. The accessory minerals are the same as described in the other massive monzodiorites.

The RMF-18-168-A is less porphyritic. The grainsize is finer and there are only few medium-size (<0.5 mm) euhedral plagioclases phenocrysts standing out from the groundmass. Other phenocrysts are poikilitic hornblende. The groundmass consists of plagioclase (~30 vol%), hornblende (~15 vol%), alkali feldspar (~15 vol%), orthopyroxene (~20 vol%), biotite (~10 vol%), and clinopyroxene (~5 vol%).

The sample RMF-18-188-A is mineralogically different from the other massive monzodiorites. The amount of clinopyroxene (~25 vol%) is higher than orthopyroxene (~10 vol%) when it is usually vice versa. This sample also lacks hornblende. Other main minerals are plagioclase (~30 vol%), alkali feldspar (~15 vol%), and biotite (~15 vol%).

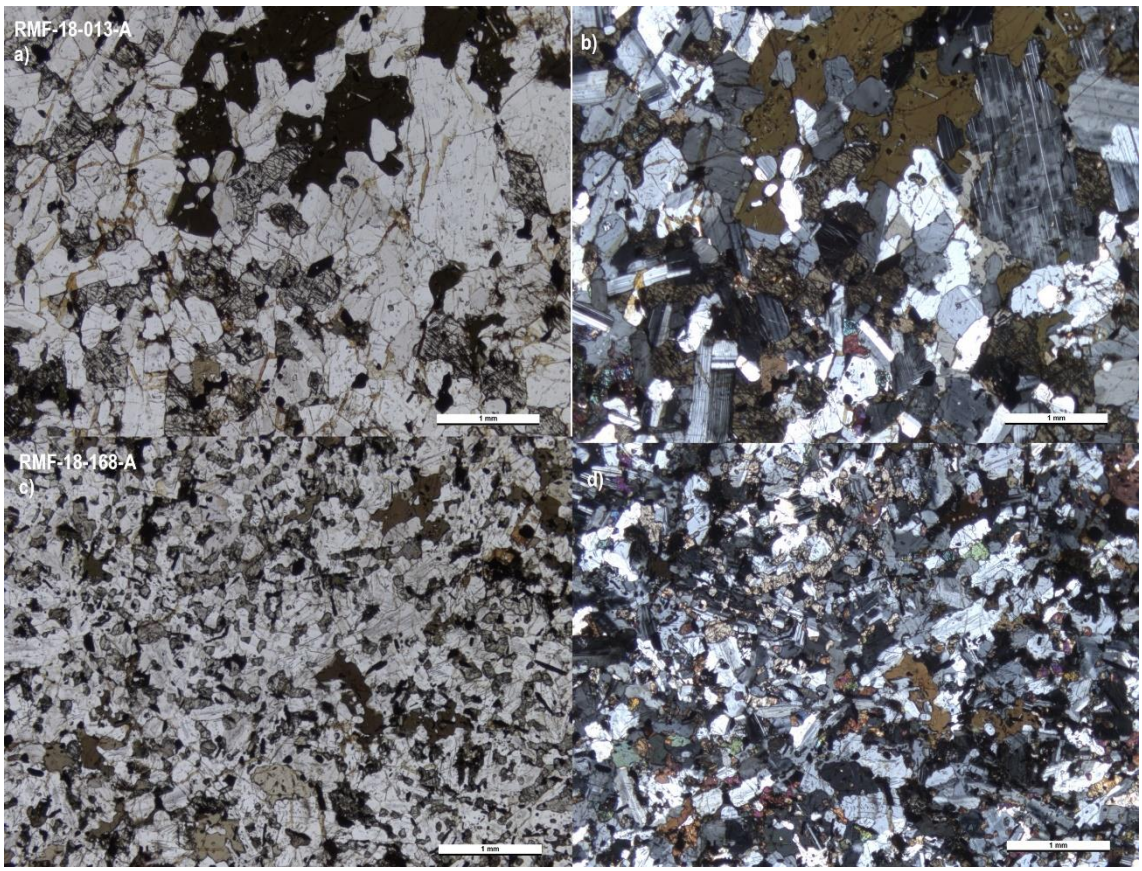

Figure 6. Photomicrograph of monzodioritic samples from Tuuliniemi (RMF-18-013-A) and Eastern part (RMF-18-168-A) showing the difference in mineral size. Photomicrographs are taken in plane-polarized (a and c) and cross-polarized (b and d) light.

4.2 Mineral chemistry of the main mineral phases of the magma interaction related rocks

In this section, the chemical composition of the main mineral phases is presented as descriptions of specific features of each set (mingling-, mixing-, and monzodiorite-set) in separate subsections. The feldspar compositions and compositional phases from all the four sets are presented in Figure 7.

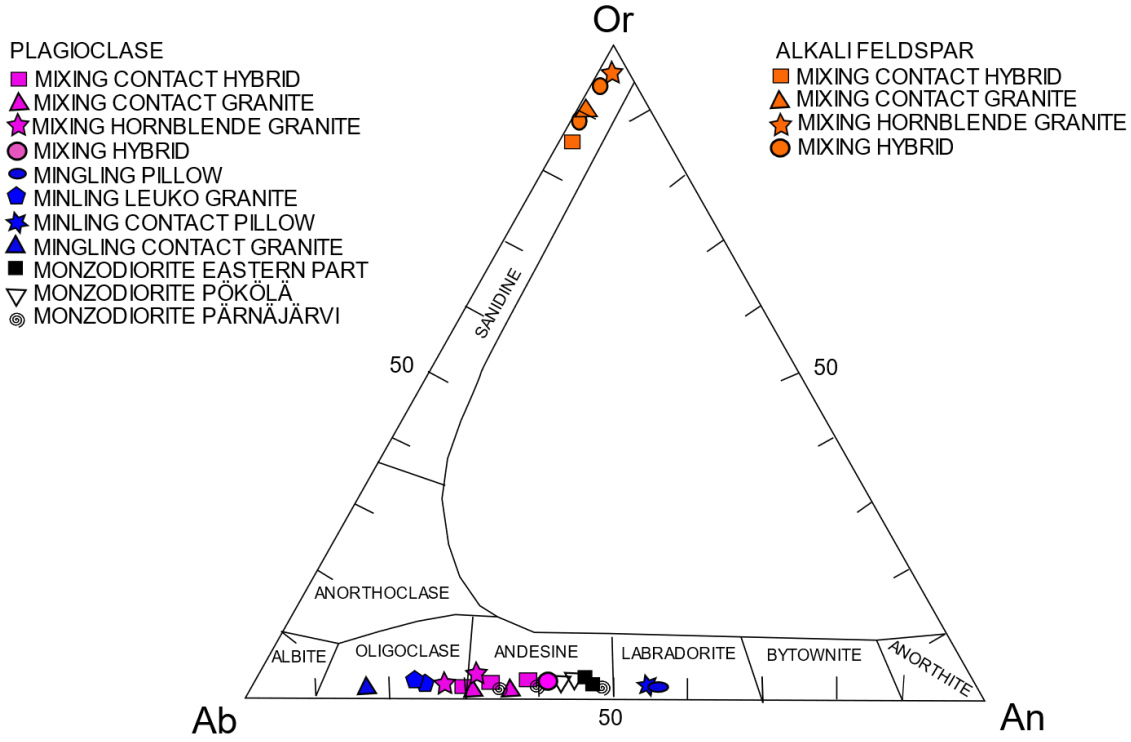

Figure 7. Ternary plot of the An-Ab-Or components combined with compositional phase diagram from the alkali feldspar analyses in the mixing set rocks and from the plagioclase analyses in rocks of the mingling, mixing, and monzodiorite sets of the Ahvenisto complex samples.

Full datasets are presented in appendices 2: a) plagioclase, b) biotite, c) hornblende, d) alkali feldspar, and e) clino- and orthopyroxene. The ferric and ferrous iron contents of biotite were estimated after Bruiyn et al. (1983). The contents of ferric and ferrous iron of pyroxene were estimated after Droop (1987).

4.2.1. Mingling set

In total, six plagioclase grains were analyzed from the mingling set: two from the center of a monzodioritic pillow (APHE-14-011.E.H1), two from the center of leucocratic vein granite (APHE-14-011.5.H3) and one grain from both sides of the contact of the monzodioritic pillow and the vein granite (APHE-14-011.5.H1). The composition of the plagioclase is An_{56} (SiO_2 = 53.1–53.6 wt%) in the monzodioritic pillow, An_{24} (SiO_2 = 61.3–62.6 wt%) in the center of the vein granite and An_{15} (SiO_2 = 63.7–66.5 wt%) in the vein granite near the contact to monzodiorite.

Two biotite grains from monzodioritic pillows, two grains from vein granite and one grain from both sides of the contact of the monzodioritic pillow and the granite vein were analyzed. Biotite from both the center and the contact in the granite vein are annite-rich with $Mg/(Mg+Fe^{2+})$ and Al^{VI} values <0.4, whereas biotite analyses from the monzodioritic pillows form another group with phlogopitic [$Mg/(Mg+Fe^{2+})$>0.4] compositions (Fig. 8).

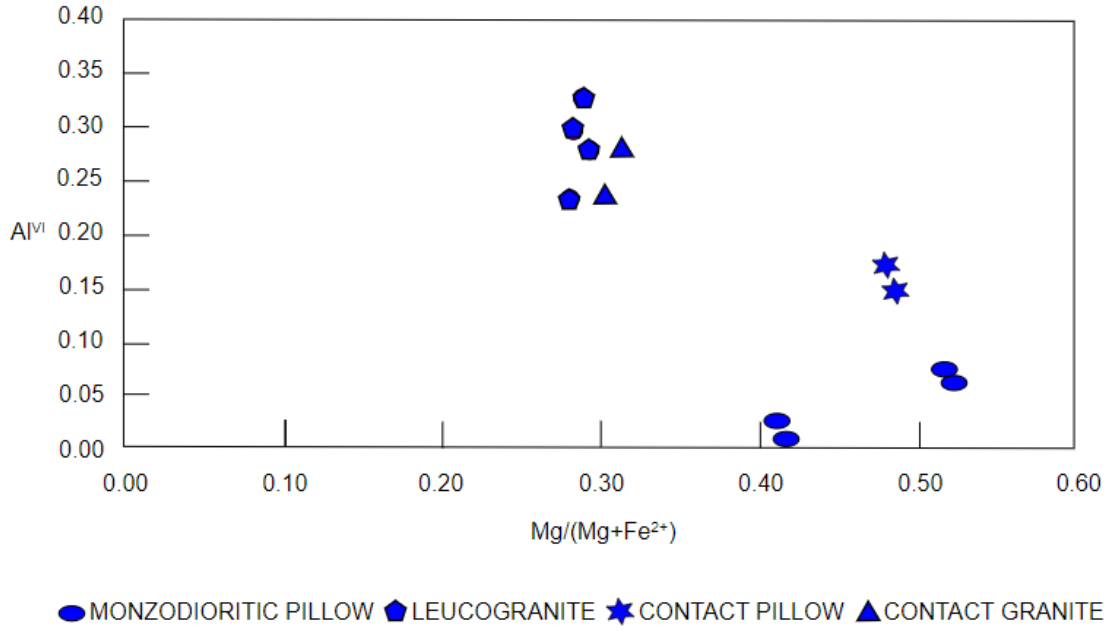

Figure 8. Biotite analyses from the rocks of the mingling set of the Ahvenisto complex on a Mg/(Mg+Fe2+) vs. Al^{VI} diagram.

4.2.2. Mixing set

From the mixing set, eight plagioclase grains (Appendix 2a) were analyzed: two from hornblende granite (RMF-15-115-B.H1), two from hybrid rock (RMF-15-115-C.H1) and four from the contact of the hornblende granite and the hybrid rock (RMF-15-115-A.H1), three grains from the granite side and one from the hybrid side.

The composition of the plagioclase is An_{28} (SiO_2 = 59.9–61.9 wt%) in hornblende granite, An_{35} (SiO_2 = 57.7–60.7 wt%) in the hybrid rock, An_{35} (SiO_2 = 58.5–59.1 wt%) in the

hornblende granite in the contact, and An_{33} (SiO_2 = 58.0–61.0 wt%) in the hybrid rock in the contact.

Compositions of the five analyzed biotite grains from the mixing set are plotted on a Mg/(Mg+Fe2+) vs. Al^{VI} diagram (Fig. 9) in which their compositions correspond to annite with both values <0.4. At the contact, the biotite composition of the hybrid changes from low Al and Mg to higher values towards the contact of the hornblende granite.

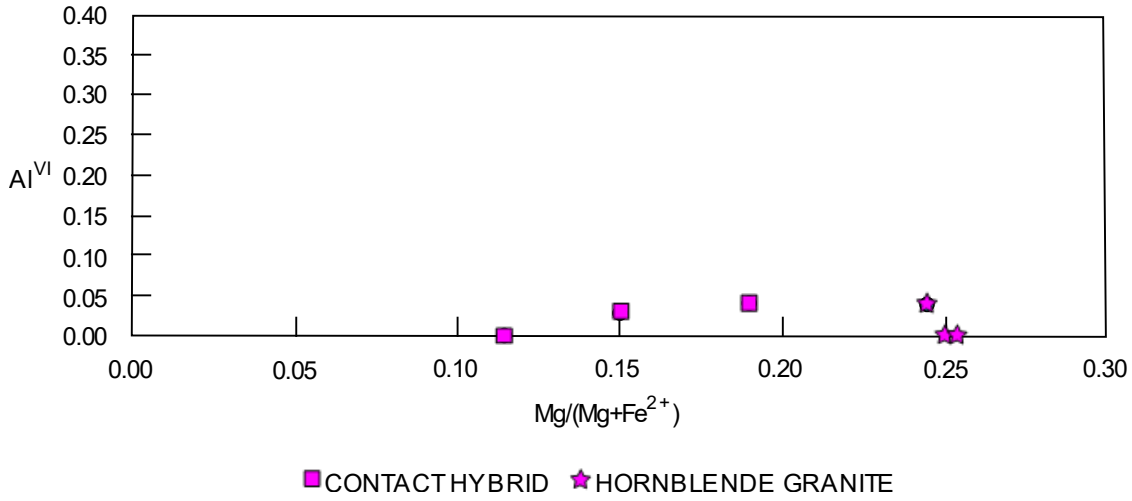

Figure 9. Biotite analyses from the rocks of the mixing set of the Ahvenisto complex plotted on a Mg/(Mg+Fe^{2+}) vs. Al^{VI} diagram.

Eight hornblende grains from the mixing set samples were analyzed (Appendix 2c): two grains both from the hornblende granite and the hybrid rock and four from the contact of the hornblende granite and the hybrid rock, three grains from the hornblende granite side and one from the hybrid side. All analyzed hornblende grains have $(Na+K)_A$>0.50, Ti<0.50, and Fe^{3+}>Al^{VI}, and are classified to the principal calcic amphibole group (Leake 1978).

Hornblende in the hybrid rock and on both sides of the contact of the hornblende granite and hybrid rock, classify to the ferro-edenitic end-member group [Fig. 10; atomic Si 6.50–6.75 and Mg/(Mg+Fe^{2+})<0.50; Leake 1978], whereas the hornblende in the hornblende granite is hastingsitic [Si 6.25–6.50 and Mg/(Mg+Fe^{2+})<0.30; Leake 1978]. The

hornblende in the hornblende granite exhibits lower $Mg/(Mg+Fe^{2+})$ values as a result of higher atomic Fe content compared to the other rock types in the mixing set.

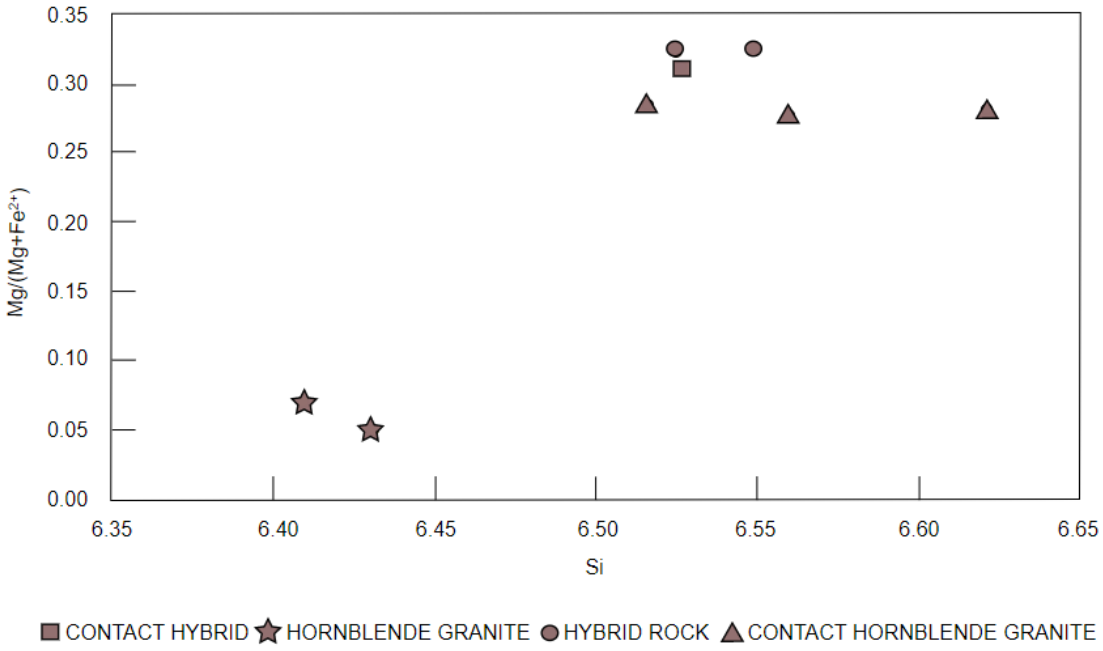

Figure 10. Hornblende analyses from the mixing set samples of the Ahvenisto complex plotted on an atomic Si vs. $Mg/(Mg+Fe^{2+})$ diagram.

Compositions of six alkali feldspar grains in the mixing set samples were analyzed (Appendix 2d): two from the hornblende granite, two from the hybrid rock and one from both sides of their contact. The composition of the alkali feldspar is Or_{95} (SiO_2 = 64.6–65.4 wt%) in hornblende granite, $Or_{89–94}$ (SiO_2 = 64.7–65.1 wt%) in the hybrid rock, Or_{85} (SiO_2 = 65.2–65.3 wt%) in the hornblende granite in the contact, and Or_{90} (SiO_2 = 65.1–65.6 wt%) in the hybrid rock in the contact.

4.2.3. Monzodiorite set

In the monzodiorite set plagioclase compositions were analyzed (Fig. 4, Appendix 2a) from two grains from eastern part (RMF-18-188-A), two grains from Pökölä area (RMF-18-077-A), and three grains from Pärnäjärvi area (RMF-15-116-A.H1) monzodiorites. The plagioclase composition in the eastern part monzodiorites is An_{45} (SiO_2 = 56.7–58.0

wt%), in Pökölä area An_{44} (SiO_2 = 56.9–58.0 wt%), and in Pärnäjärvi area An_{37} (SiO_2 = 56.6–60.4 wt%).

In total, 15 grains of pyroxenes were analyzed from the monzodiorite set: two orthopyroxene (opx) and two clinopyroxene (cpx) from the eastern part, three orthopyroxene and three clinpyroxene from Pökölä area, and three orthopyroxene and two clinopyroxene from Pärnäjärvi area (Appendix 2e).

Pyroxene end-members were calculated after Morimoto (1988) by normalizing Ca+Mg+Fe_{Σ} (Fe_{Σ} = Fe^{2+}+Fe^{3+}+Mn^{2+}) to 100. The end-members are presented in Wo ($CaSiO_3$), En ($MgSiO_3$), and Fs ($FeSiO_3$) diagram for Ca-Mg-Fe pyroxene classification in Figure 11.

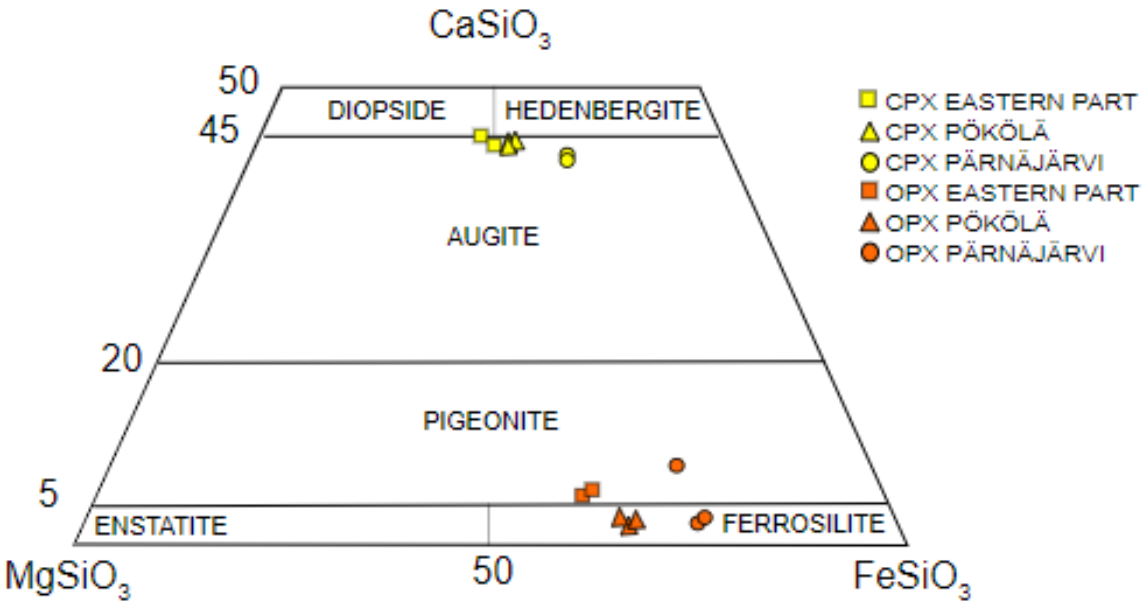

Figure 11. Classification diagram for Ca-Mg-Fe pyroxenes in the monzodiorites of the Ahvenisto complex after Morimoto (1988).

The orthopyroxene compositions mainly plot in the ferrosilite field (Fig. 11). The ortopyroxene from the eastern part have the composition of $En_{35}Fs_{59}Wo_6$ and from Pökölä area $En_{33}Fs_{65}Wo_2$. In Pärnäjärvi area, the orthopyroxene composition is more Fe-rich than in the other study areas and the amount of Ca varies ($En_{24}Fs_{74}Wo_3$–$En_{24}Fs_{68}Wo_9$).

Clinopyroxene compositions from the eastern part ($En_{28}Fs_{28}Wo_{44}$) and Pökölä area ($En_{26}Fs_{30}Wo_{44}$) are similar as well, whereas clinopyroxene from Pärnäjärvi area ($En_{20}Fs_{38}Wo_{42}$) is more Fe-rich compared to them (Fig. 11). The clinopyroxene analyses mainly plot into the augite field, except for one sample (RMF-18-188-A) from the eastern part, which plots on the diopside-augite divide.

A multiplot of SiO_2 vs. Al_2O_3, MgO, CaO and FeO^{tot} of the orthopyroxene analyses is presented in Figure 12. The orthopyroxenes of the different study areas form three distinguishable groups when compared on SiO_2 vs. MgO and FeO^{tot}. The orthopyroxene in the easter part of the Ahvenisto complex have higher Mg/Fe compared to the other study areas. Orthopyroxene from the Pärnäjärvi study area is comparatively higher in Fe.

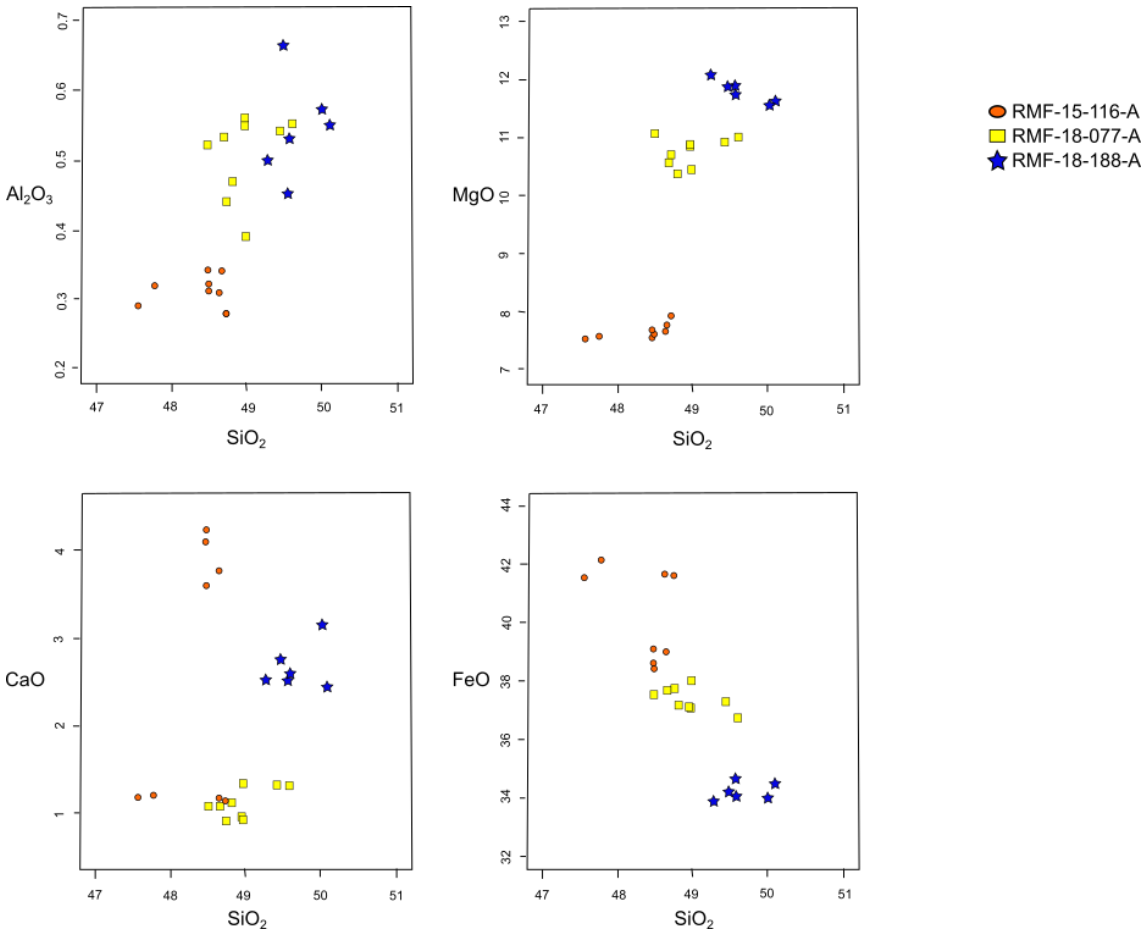

Figure 12. Multiplot of SiO_2 vs. Al_2O_3, MgO, CaO and FeO^{tot} from the orthopyroxenes in the monzodiorites of the Ahvenisto complex. The samples are from Pärnäjärvi (116-A), Pökölä (077-A), and the eastern part (188-A).

Multiplot of SiO_2 vs. Al_2O_3, MgO, CaO and FeO^{tot} of clinopyroxenes is presented in Figure 13. Also in the clinopyroxenes, same three groups can be identified, when compared in SiO_2 vs. MgO and FeO^{tot}. The clinopyroxenes in the eastern part have higher Mg compared to Fe and in the Pärnäjärvi area the relation is the opposite.

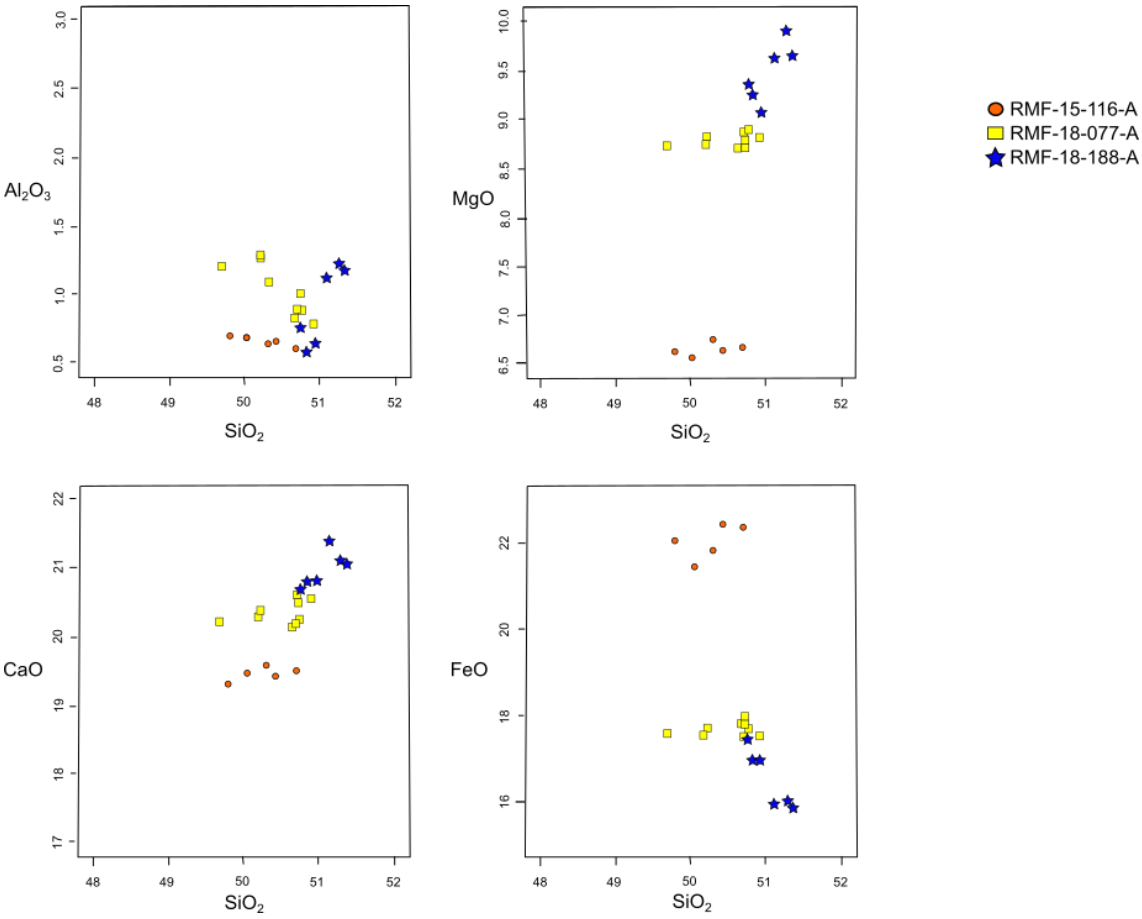

Figure 13. Multiplot of SiO_2 vs. Al_2O_3, MgO, CaO and FeO^{tot} from the clinopyroxenes in the monzodiorites of the Ahvenisto complex. The samples are from Pärnäjärvi (116-A), Pökölä (077-A), and the eastern part (188-A).

4.3. Geothermobarometry

The purpose of the study was to test the suitability of geothermobarometric methods for the rock types related to the different magma interaction structures and to evaluate crystallization pressures and temperatures of the pertinent magmas. The most suitable geothermobarometers were chosen to use in this study to best represent the minerals and

compositions common to the rock types related to the magma interaction structures in the Ahvenisto complex.

4.3.1. Hornblende-plagioclase thermobarometry

Many of the amphibole related barometers are based only on the total aluminum content. The validity of these barometers has been challenged in many studies (e.g., Salonsaari 1995), for not being accurate enough, and for this reason, Blundy and Holland (1990) hornblende-plagioclase thermobarometer (Table 3) and Holland and Blundy (1994) hornblende-plagioclase thermobarometers A and B (Table 4), were chosen for this study to study the crystallizing temperatures in the mixing process.

Table 3. Hornblende-plagioclase thermobarometer after Blundy and Holland (1990) for the rocks of the Ahvenisto complex.

		Hornb		Plag		T (°C)		
Sample ID	Rock	[a]N	[b]Si	[a]N	[c]Ab	100 Mpa	300 Mpa	500 Mpa
RMF-15-115-A.H1	Hornblede granite contact	4	6.579	6	0.658	815	785	754
	Hybrid rock contact	4	6.526	4	0.640	833	802	771
RMF-15-115-B.H1	Hornblede granite	2	6.409	2	0.681	846	815	783
	Hornblede granite	2	6.430	2	0.714	831	800	769
RMF-15-115-C.H1	Hybrid rock	2	6.525	2	0.584	853	821	790
	Hybrid rock	2	6.549	2	0.674	817	787	756

[a]number of analyses in average composition

[b]Si in hornblende (pfu)

[c]albite content of plagioclase

For Blundy and Holland (1990) hornblende-plagioclase thermobarometer:

$$T(°C) = [(0.677P - 48.98 + Y)/(-0.0429 - 0.008314lnK)] - 273.15 \qquad (2)$$

where K = [(Si – 4)/(8 – Si)] and Y = 0 for $X_{ab} > 0.5$.

For the samples in the hornblende granite-hybrid rock contact, the Blundy and Holland (1990) hornblende-plagioclase thermobarometer gives temperatures of 815–833°C at 100 MPa, 785–802°C at 300 MPa, and 754–771°C at 500 MPa, with the highest temperatures

being at the hybrid rock side of the contact. Temperatures from the hornblende granite samples vary between 831–846°C at 100 MPa, 800–815°C at 300 MPa, and 769–783°C at 500 MPa. The hybrid rock samples give temperatures of 817–853°C at 100 MPa, 787–821°C at 300 MPa, and 756–790°C at 500 MPa.

Table 4. Hornblende-plagioclase thermobarometers A and B after Holland and Blundy (1994) for the rocks of the Ahvenisto complex.

		TA (°C)			TB (°C)		
Sample ID	Rock	100 MPa	300 MPa	500 MPa	100 MPa	300 MPa	500 MPa
RMF-15-115-A.H1	Hornblede granite contact	825	801	778	797	802	806
	Hybrid rock contact	829	807	784	810	815	820
RMF-15-115-B.H1	Hornblede granite	863	837	812	815	819	823
	Hornblede granite	817	796	775	783	788	793
RMF-15-115-C.H1	Hybrid rock	862	837	812	838	842	846
	Hybrid rock	813	792	770	790	795	800

TA = thermobarometer A

TB = thermobarometer B

For Holland and Blundy (1994) hornblende-plagioclase thermobarometers A and B:

$$T_A = \frac{-76.95 + 0.79P + Y_{ab} + 39.4X_{Na}^{A} + 22.4X_{K}^{A} + (41.5 - 2.89P) * X_{Al}^{M2}}{-0.0650 - R * ln\left(\frac{27 * X_{\square}^{A} X_{Si}^{T1} * X_{ab}^{plag}}{256 * X_{Na}^{A} * X_{Al}^{T1}}\right)} \quad (3)$$

where cm = Si + Al + Ti + Fe^{3+} + Fe^{2+} + Mg + Mn – 13.0, X_{Si}^{T1} = (Si – 4)/4, X_{Al}^{T1} = (8 – Si)/4, X_{Al}^{M2} = (Al + Si – 8)/2, X_{K}^{A} = K, $X_{\square}^{A}$ is 3 – Ca – Na – K – cm, X_{Na}^{A} = Ca + Na + cm – 2, and Y_{ab} = 0 for X_{ab} > 0.5. T is temperature in Kelvins, P is the pressure in kbar, and R is the gas constant.

$$T_B = \frac{78.44 + Y_{ab-an} - 33.6X_{Na}^{M4} - (66.8 - 2.92P) * X_{Al}^{M2} + 78.5X_{Al}^{T1} + 9.4X_{Na}^{A}}{0.0721 - R * ln\left(\frac{27 * X_{Na}^{M4} * X_{Si}^{T1} * X_{an}^{plag}}{64 * X_{Ca}^{M4} * X_{Al}^{T1} * X_{ab}^{plag}}\right)} \quad (4)$$

where cm is Si + Al + Ti + Fe^{3+} + Fe^{2+} + Mg + Mn – 13.0, X_{Si}^{T1} = (Si – 4)/4, X_{Al}^{T1} = (8 – Si)/4, X_{Al}^{M2} = (Al + Si – 8)/2, X_{Na}^{A} = Ca + Na + cm – 2, X_{Na}^{M4} = (2 – Ca – cm)/2, X_{Ca}^{M4} = Ca/2, and $Y_{ab–an}$ = 3.0 kJ for X_{ab} > 0.5. T is temperature in Kelvins, P is the pressure in kbar, and R is the gas constant.

For Holland and Blundy (1994) hornblende-plagioclase thermobarometer A, the samples in the hornblende granite-hybrid rock contact gives temperatures of 825–829°C at 100 MPa, 801–807°C at 300 MPa, and 778–784°C at 500 MPa. Holland and Blundy (1994) hornblende-plagioclase thermobarometer B for the same samples give temperatures of 797–810°C at 100 MPa, 802–815°C at 300 MPa, and 806–820°C at 500 MPa. For both thermobarometers the highest temperatures are calculated from the hybrid rock side of the contact.

Temperatures from the hornblende granite samples vary between 817–863°C at 100 MPa, 796–837°C at 300 MPa, and 775–812°C at 500 MPa for the thermobarometer A, and between 783–815°C at 100MPa, 788–819°C at 300 MPa, and 793–823°C at 500 MPa for the thermobarometer B. The thermobarometer A for the hybrid rock samples give temperatures of 813–862°C at 100MPa, 792–837°C at 300 MPa, and 770–812°C at 500 MPa. Thermobarometer B gives temperatures of 790–838°C at 100 MPa, 795–842°C at 300 MPa, and 800–846°C at 500 MPa for the hybrid rocks.

4.3.2. Two-pyroxene thermometry

Different two-pyroxene thermometers were tested on the monzodioritic rocks of the Ahvenisto complex, but only few of them were suitable for this study. For example, the application by Putirka (2008) cannot be used because of the mineralogical nature of the mafic minerals in the samples being very iron-rich. The Mg# would need to be > 0.75 for

this thermometer, but in the sample rocks Mg# is lower varying from 0.35 to 0.53. Two-pyroxene thermometers T1 from Wood and Banno (1973) and T2 from Wells (1977), were used in the calculations to study the crystallization temperatures of the monzodioritic rocks. The results are presented in Table 5.

Table 5. Two-pyroxene thermometers T1 (Wood and Banno 1973) and T2 (Wells 1977) from the monzodioritic rocks of the Ahvenisto complex.

		CPX		OPX		T1 (°C)	T2 (°C)
Sample ID	Location	X_{Fe}^{cpx}	$a_{Mg2Si2O6}^{cpx}$	X_{Fe}^{opx}	$a_{Mg2Si2O6}^{opx}$		
RMF-18-188-A	Eastern part	0.476	0.313	0.620	0.485	957	1110
		0.503	0.288	0.615	0.506	941	1082
RMF-18-077-A	Pökölä	0.524	0.264	0.667	0.407	940	1083
		0.521	0.262	0.657	0.426	936	1075
		0.531	0.262	0.655	0.431	936	1074
RMF-15-116-A.H1	Pärnäjärvi	0.647	0.154	0.753	0.219	926	1052
		0.649	0.155	0.737	0.220	930	1061

cpx = clinopyroxene, opx = orthopyroxene

T1 = Wood and Banno (1973)

T2 = Wells (1977)

For Wood and Banno (1973) two-pyroxene thermometer:

$$T1 = \frac{-10202}{ln\left(\frac{a_{Mg_2Si_2O_6}^{cpx}}{a_{Mg_2Si_2O_6}^{opx}}\right) - 7.65X_{Fe}^{Opx} + 3.88\left(X_{Fe}^{Opx}\right)^2 - 4.6} \quad (5)$$

where $a_{Mg_2Si_2O_6} = \left(\frac{Mg^{2+}}{Ca^{2+}+Mg^{2+}+Fe^{2+}+Mn^{2+}+Na^{+}}\right)_{M2} * \left(\frac{Mg^{2+}}{Fe^{3+}+Fe^{2+}+Al^{3+}+Ti^{4+}+Cr^{3+}+Mg^{2+}}\right)_{M1}$

and T is temperature in Kelvins.

For Wells (1977) two-pyroxene thermometer:

$$T2 = \frac{7341}{3.355 + 2.44X_{Fe}^{Opx} - lnK} \quad (6)$$

where T is in Kelvins.

For Wood and Banno (1973) two-pyroxene thermometer (T1), the samples from the monzodioritic rocks from the Eastern part gives temperatures of 941–957°C, from Pökölä 936–940°C, and from Pärnäjärvi 926–930°C. Wells (1977) two-pyroxene thermometer (T2) for the same samples give results of 1082–1110°C from the Eastern part, 1074–1084°C from Pökölä, and 1052–1061°C from Pärnäjärvi.

5. DISCUSSION

5.1. Comparisons of mineral compositions

5.1.1. Mingling set

Biotite in the leucogranite and in the contact of the granite vein towards the monzodioritic pillow are classified as annite with Al^{VI} from 0.24 to 0.33 and $Mg/(Mg+Fe^{2+})$ from 0.28 to 0.31. Respectively, both within and in the contact of the monzodioritic pillow, biotite is classified as phlogopite with Al^{VI} from 0.01 to 0.17 and $Mg/(Mg+Fe^{2+})$ from 0.41 to 0.52. In addition to these two populations, biotite composition in the mingling-structured rocks is also somewhat spatially controlled (Fig. 8). Biotite Al content clearly increases from the center of the monzodioritic pillow towards the contact and decreases slightly from the center of the leucocratic vein granite towards the contact. Variation in the $Mg/(Mg+Fe^{2+})$ ratio is not as clear. The compositional differences are also visible in thin sections as there are two distinct generations of biotite found in the mingling-related thin section samples.

Plagioclase analyzed from the mingling set (Fig. 7) exhibits a wide compositional change because of the difference in the nature of the rocks. Samples from the monzodioritic pillow are clearly more Ca rich with An_{56} (labradorite). The granitic samples are more albitic in composition with An_{24} within the vein and An_{15} in the granite contact. Both of these classify as oligoclase. All plagioclase analyses have very low K values with their Or component being mostly less than 2 mol%.

5.1.2. Mixing set

The An-Ab-Or components and the plagioclase compositions analyzed from the mixing set are presented in Figure 7. The compositional range of the plagioclase in this set is $An_{28–35}$. The Or content is low being under 2 mol%. In the An-Ab-Or ternary diagram plagioclase composition varies through mixing from the most Na-enriched end-member, in the hornblende granite via the contact granite to contact hybrid and finally to the hybrid rock, which is the most Ca-enriched end-member. Most of the plagioclase samples are classified as andesine but couple of the samples are oligoclasic. Composition of the plagioclase is similar to the Jaala-Iitti complex reference samples studied by Salonsaari (1995). In Jaala-Iitti the composition of plagioclase in hybrid rock varies between $An_{28–42}$ and in hornblende granite from An_{20} to An_{35}.

Walker and Skelhorn (1966) point out that the composition of the alkali-feldspar phenocrysts in hybrid rocks provides important evidence of their origin. The composition of the studied alkali-feldspar (Fig. 7) shifts from orthoclase to more albitic composition as analyzed from their suggested mixing origin of hornblende granite towards the contact and the hybrid rock. This implies that K in the alkali-feldspars is slightly replaced by Na due to effects from the mixing process. All samples are classified as sanidine by the phase composition. In Jaala-Iitti samples studied by Salonsaari (1995) the alkali-feldspar from the hornblende granite and the hybrid rock have $Or_{80–95}$. The alkali-feldspars from the similar rocks of Ahvenisto complex plot to the same compositional range of $Or_{89–95}$.

Salonsaari (1995) emphasizes that in theory, when two magmas have formed a completely hybridized rock, there should not be any signals of either of the end-members left. As strong evidence of hybridization, the compositions of the minerals, which were crystallized after possible magma mixing, like amphibole and biotite, should be identified and analyzed. Biotite analysis from the mixing set is presented in Figure 9. At the contact of the hybrid rock and hornblende granite, the biotite composition changes from low Al and Mg to higher values from the contact towards the hornblende granite. Biotite is classified as annite with Al^{VI} 0.00–0.04 and $Mg/(Mg+Fe^{2+})$ 0.11–0.19 in contact granite and 0.25–0.26 in hybrid rock. Salonsaari (1995) concluded that biotite in Jaala-Iitti complex are also classified as annite and reported similar values of $Mg/(Mg+Fe^{2+})$ <0.20

in granites and > 0.20 in hybrid rock types. The $Fe^{2+}/(Fe^{2+}+Mg)$ value in the biotite samples from Ahvenisto complex varies from 0.77 to 0.90. Elliott (2001) analyzed mineral chemistry of Wiborg batholith, and the results show similar values for biotite. The reported compositions were remarkably iron-enriched with $Fe^{2+}/(Fe^{2+} + Mg)$ ranging from 0.78 to 1.00.

The mineral chemistry analyzed from the hornblende of the mixing set (Fig. 10) shows a continuing distribution of Mg and Fe phases. The hornblende in the hornblende granite shows lower atomic Mg content compared to the other rock types in the mixing set. Contrary to biotite, the composition of the hornblende changes to higher Mg values from hornblende granite towards the contact and the hybrid rock. The $Fe^{2+}/(Fe^{2+}+Mg)$ value in the hornblende samples varies between 0.67 to 0.94 with hornblende in the hornblende granite reaching the highest values. Elliott (2001) also reported amphibole to be especially iron-rich with $Fe^{2+}/(Fe^{2+}+Mg)$ variation from 0.72 to 0.95.

5.1.3. Monzodiorite set

From the monzodiorite set plagioclase compositions were analyzed and the results are presented in Figure 7. All samples are classified as andesine with $An_{37–45}$. The samples from the monzodiorites of Pärnäjärvi show more variation in composition compared to the samples from Pökölä and eastern part of the Ahvenisto complex.

Mineral composition and classification of the analyzed pyroxene samples are presented in Figure 11. The composition of orthopyroxene is mainly ferrosilite but samples from the eastern part are classified as pigeonite. The clinopyroxene mainly plot into the augite field, except for one sample from the eastern part, which plots onto the line of the diopside field. Comparing both pyroxenes (Figs. 12 and 13), three groups can be separated by their mineral chemistry and location. The monzodiorite from Pärnäjärvi is more iron-rich than monzodiorites from other areas and, respectively the samples from the eastern part are more magnesian in composition compared to other samples. The monzodiorite samples from Pökölä are compositionally between the other two localities.

Fred et al. (2020) reported mineral compositions for three different rock types in the Ahvenisto complex: olivine monzodiorites, olivine-bearing anorthositic rocks, and

apatite–oxide–gabbronorite. The plagioclase samples from the apatite–oxide–gabbronorite group are classified as andesine and An_{40-43}. Also, pyroxene analysis from the apatite-oxide-gabbronorite classify mainly as ferrosilite and augite and sample points settle close to same spots as pyroxenes analyzed in Figure 11. There are clear similarities in the analyzed mineral chemistry of the apatite–oxide–gabbronorite group and the monzodiorite set. Regardless of that, Fred et al. (2020) state, that even the apatite–oxide–gabbronorite of the Ahvenisto complex have relatively evolved composition, they are not categorized as monzodioritic rocks but rather represent late-stage cumulates. Since the mineral chemistry is similar this could lead to the conclusion that the analyzed monzodiorites also have crystallized in the later stages of the evolution of the Ahvenisto complex rather than during the earlier emplacement of the complex.

5.2. Previous estimates for the emplacement conditions of the Wiborg batholith magmas

The emplacement conditions of the magmas that formed the Wiborg batholith and related intrusions have previously been examined chiefly based on the Al-in-hornblende barometer (e.g., Salonsaari 1995, Elliott 2001). From the results of these studies, it is evident that the evolution of the Wiborg batholith and related intrusions may not be identical. According to Salonsaari (1995) and Elliott (2001), one problem in determining the intrusion mechanics of the Wiborg batholith in detail has been, that the calibration of the Al-in-hornblende barometer is not robust for the observed mineral compositions. Despite the popularity of the Al-in-hornblende barometer, problems in the reliability of its applications have been recognized in Fe-enriched and high Fe^{2+}/Fe^{3+} conditions. Also the compositional complexity of the amphibole group presents a major challenge for determining the barometer parameters and the mechanism that controls the aluminum content in hornblende still remains unclear (e.g., Hollister et al. 1987, Ague 1997, Putirka 2016).

Salonsaari (1995) suggested that the wide range in the observed emplacement pressures for Wiborg rocks could result from the change in the composition of the amphiboles due to cooling or reheating of the magmas during their evolution. According to Elliott (2001), Al-in hornblende barometer used in these studies was not calibrated to be used with rocks

that have high (>0.65) Fe/(Fe+Mg) ratios. Salonsaari (1995) concluded, that the granites in the Jaala-Iitti complex crystallized at temperatures of 850–650 °C and the hybrids at 900–750°C. He also assumed in his studies that the emplacement of the complex took place at relatively shallow crustal levels, at pressures less than 200 MPa. The amphibole geobarometers yielded a range of pressures from 100 to 500 MPa, which leaves some uncertainty as to the reliability of the result. Elliott (2001), however, suggested that the largest part of the rapakivi granites in the Wiborg batholith crystallized at somewhat greater pressures of 400 MPa and some granites even at the pressure of 490 MPa.

Kivisaari (2015) and Heinonen et al. (2020) utilized the Al-in-orthopyroxene geobarometer to study the crystallization pressure of high-aluminum orthopyroxene megacrysts (HAOM) in the Ahvenisto complex and estimated that the complex was emplaced at around 200 MPa (<10 km depth). Additionally, the results from the HAOM studies support the evidence of polybaric magmatic evolution of the Ahvenisto complex. This evidence suggests that the shallow emplacement of the magmas was preceded by several crystallization stages at depths of down to 35–40 km.

5.3. Geothermobarometric inferences

5.3.1. Hornblende-plagioclase thermobarometry

Blundy and Holland (1990) hornblende-plagioclase thermobarometer (Table 3) and Holland and Blundy (1994) hornblende-plagioclase thermobarometers A and B (Table 4) were utilized in the hornblende-plagioclase thermobarometry. The compiled results are illustrated and compared to those reported for the Jaala-Iitti complex by Salonsaari (1995) in Figure 14.

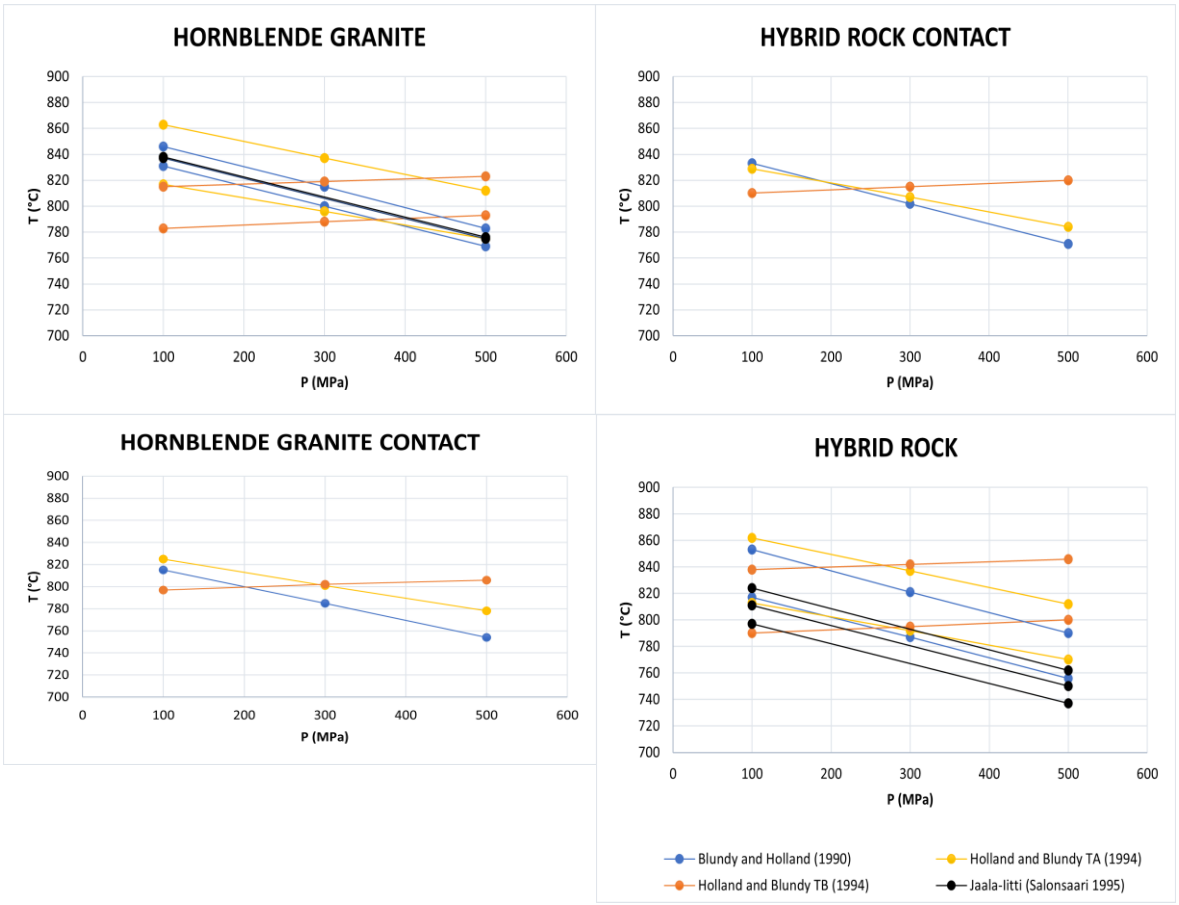

Figure 14. The crystallization temperatures calculated for the mixing-related rocks from the hornblende-plagioclase thermobarometers at 100, 300, and 500 MPa. Thermometry results reported by Salonsaari (1995) for similar rock types in the Jaala-Iitti complex are shown for comparison.

Pressure conditions of 100 MPa, 300 MPa, and 500 MPa were considered in the thermometric calculations. Recent high-aluminum orthopyroxene megacryst (HAOM) research (Kivisaari 2015, Heinonen et al. 2020) for the crystallization conditions of the Ahvenisto complex concluded that the best estimation for the emplacement pressure is around 200 MPa. For this reason, the temperature results calculated between 100 MPa and 300 MPa will be discussed here in more detail and considered as the best estimates.

Blundy & Holland (1990) geothermometer was also used in the research concerning the crystallization temperatures of the Jaala-Iitti complex (Salonsaari 1995) and the Wiborg batholith (Elliott 2001). Reported temperatures in Jaala-Iitti at 100 MPa for the hornblende granite are 837–838°C and 797–824°C for the hybrid rock. The results fit to the same range with the temperatures of the similar rocks in the Ahvenisto complex in

this study between 100 MPa and 300 MPa (Fig. 14). Suggested crystallization for the Wiborg batholith took place at about ~740°C in pressure range of 250–540 MPa.

For all of the thermobarometers, the highest temperatures are calculated from the hybrid rock side of the contact and at 100 MPa in Blundy and Holland (1990), and Holland and Blundy (1994) TA, but at 300 MPa in thermobarometer TB. The results show that Holland and Blundy (1994) TA and TB are calibrated to give reversed temperature gradients compared to each other. The temperature change in each individual sample is very consistent and small when moving from 100 MPa to 300 MPa, and even to 500 MPa. In Table 3 the change is ca. -15°C per 100 MPa, and in Table 4 the change is ca. -10°C (TA) and ca. +2.5°C (TB) per 100 MPa. This shows that the thermometers are not very sensitive to pressure.

Blundy and Holland (1990) concluded that the uncertainty for the hornblende-plagioclase thermobarometer is ±75°C. Holland and Blundy (1994) report the uncertainty of the results for the hornblende-plagioclase thermobarometers A and B to be ±35–40°C. It is emphasized that the uncertainty is very sensitive to iron-rich amphiboles as their ferric/ferrous estimation scheme may lead to very different oxidation states compared to the calibration dataset.

5.3.2. Two-pyroxene thermometry

Two-pyroxene thermometers T1 (Wood and Banno 1973) and T2 (Wells 1977) were used to calculate the equilibrium temperatures of coexisting ortho-and clinopyroxene in the Ahvenisto complex massive monzodiorites. The results are presented in Table 5 and illustrated in Figure 15.

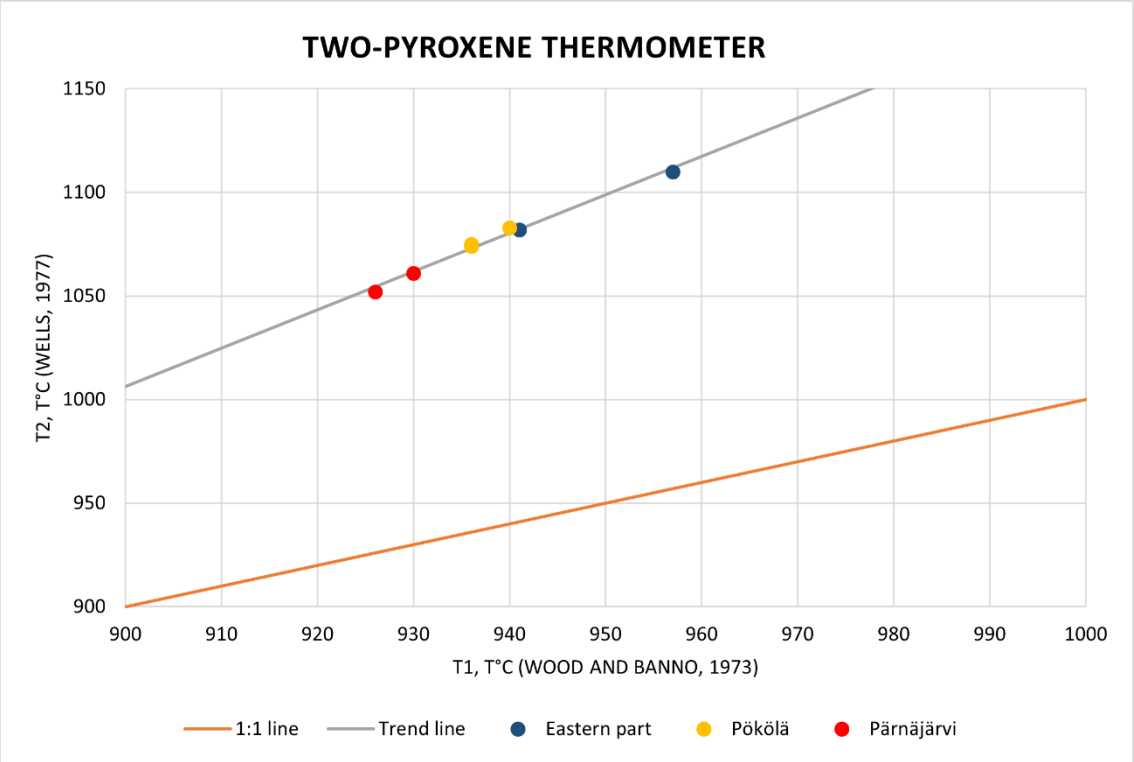

Figure 15. The crystallization temperatures for the monzodiorite set from two-pyroxene thermometers.

The Wells (1977) two-pyroxene thermometer (T2) gives higher temperatures for all studied monzodiorite samples than the T1 thermometer (Wood and Banno 1973). Largest difference is in the eastern part with +153°C and smallest in Pärnäjärvi with +126°C. In Pökölä the difference is about +140°C. Although, there is variation in the calculated temperatures, they seem to follow the same trend line (Figure 15) and confirm the fact, which was based on the base of the mineral chemistry of the monzodiorite set, for Pökölä monzodiorite being settled between the other two monzodiorites also by the crystallization temperature.

Wells (1977) highlights that the deviations between the results of Wells (1977) two-pyroxene thermometer and Wood and Banno (1973) two-pyroxene thermometer are largest at low values of X_{Fe}^{Opx}, at low to moderate temperatures (<1100°C), and with Mg-rich composition. The accuracy of the geothermometers (Wood and Banno 1973, Wells 1977) is presented to be within ±70°C. Other authors (e.g., Fonarev and Graphchikov 1982, Lindsey and Andersen 1983, Rietmeijer 1984,) claim for the results from Wood and Banno (1973) and Wells (1977) two-pyroxene thermometer to be 100–185°C too high.

Salonsaari (1995) presented proof of different stages of crystallization for pyroxenes in the Jaala-Iitti complex which creates difficulties for application of pyroxene thermometers. As an estimation for the lowest possible crystallization temperature of the pyroxenes with similar mineral chemistry, Lindsey pyroxene thermometry (1983) was used, and resulted 825°C. In Table 5, the results are 101–132°C higher with T1 and 227–285°C higher with T2 compared to the lowest possible by Lindsey (1983). The temperatures are getting closer if the results in T1 and T2 are corrected with the suggested 100–185°C error.

5.3.3. Inferences for the modes of magma interaction

As presented in Figure 4, Fred (2017) calculated melt viscosity models for a) mingling, and b) mixing related rocks of the Ahvenisto complex. In order to study the relative viscosities in different interaction cases, Fred (2017) used calculated liquidus temperatures as inputs for the viscosity models. Below (Fig. 16), the temperatures from the geothermobarometry calculations in this study are combined with the viscosity models and compared to the previous inferences based on liquidus temperatures.

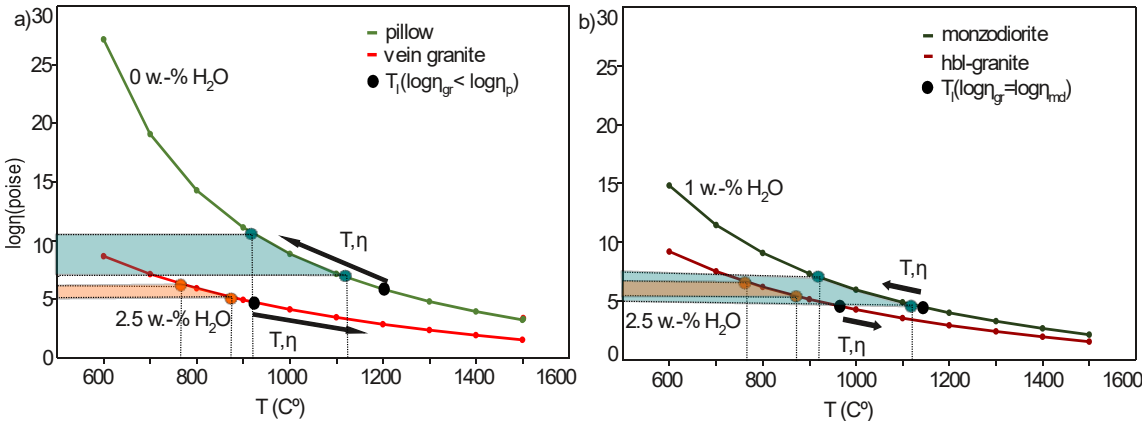

Figure 16. An illustration of the reference temperatures from the geothermobarometry combined with the melt viscosity models for a) mingling of monzodioritic pillows (at 0 wt% H_20) and granitic veins (at 2.5 wt% H_20) and b) mixing of massive monzodiorite (at 1.0 wt% H_20) and hornblende granite (at 0 wt% H_20). Also illustrated are the liquidus temperatures (T_l) and corresponding T-η evolution caused by magma interaction sketched by Fred (2017). Figure is modified from Fred (2017).

The previous conclusions drawn from the melt viscosity models (Fred 2017) are supported, and even strengthened by the new results. In the mingling case (Fig. 16a), the

monzodioritic pillow and the vein granite have clearly different viscosities and, thus, are not able to mix but commingle. Respectively in the mixing case (Fig. 16b) the massive monzodiorite and hornblende granite show similar range of viscosities at the thermobarometer-derived temperatures. This suggests that they can mix and form a hybrid rock. It is, however, important to notice, that for both of the melt viscosity models, the reference temperatures are calculated for massive monzodiorites (two-pyroxene thermobarometers) and hornblende granite (hbl-pl thermobarometers). Monzodioritic pillows and granitic veins were not used in geothermobarometric calculations. The temperature results from the mixing-related rocks are most likely close enough to be used as an implication also for the mingling-related rocks but most likely represent the minimum temperatures for that comparison.

6. CONCLUSIONS

It is evident, that the evolution of the Wiborg rapakivi batholith has occurred through several magmatic phases. Some of these phases have affected the Ahvenisto complex rocks by mixing and mingling. The changes are also recognized in the mineral chemistry of the rocks. The results of this study seem to support the mixing hypothesis developed by Fred (2017; see also Fred et al. 2019). The hornblende granite represents the most primitive granitic phase in the mixing set and the composition of the minerals change as the mixing proceeds towards the final hybrid rock.

For the monzodiorite set, the mineral chemistry reveals that the monzodiorites from different areas of the Ahvenisto complex have distinguished features and they can be separated by their composition. The mineral chemistry of the analyzed monzodiorites supports the geochemical evolutionary trend of monzodioritic rocks of the complex from olivine monzodiorite through pillow-type monzodiorite to massive monzodiorite suggested by Fred et al. (2019). The studied monzodiorites belong to the later stage more evolved compositions and, thus, most likely yield the minimum crystallization conditions (P-T) for the Ahvenisto monzodioritic magma series.

Although there is some deviation in the conclusions drawn from the results of different geothermobarometers, the majority of the studies suggest that the emplacement of the Ahvenisto complex took place at lower pressures (~200 MPa) and at relatively shallow levels (under 7 km) in the crust. The hornblende-plagioclase thermobarometers suggest similar crystallization temperatures for the Ahvenisto complex as reported in the earlier studies from the other parts of the Wiborg batholith. The crystallization of the mixing related rocks took place ~790–860°C and pressure has had only a minor impact on the temperature. This implies that the temperatures derived from the hornblende-plagioclase thermobarometers are applicable to the studied samples.

Two-pyroxene thermometers show clear regional difference for the crystallization temperatures of the Ahvenisto monzodioritic rocks. According to reference literature, there is more variation and uncertainty on the liability of the results. The uncertainty is mainly explained by the mineral chemistry of the mafic silicate minerals in the Ahvenisto complex rocks being very iron-rich and outside the calibration standards of the geothermobarometers. The temperatures from two-pyroxene thermometers to be higher than the temperatures from hornblende granite thermobarometers is natural. Being more mafic, the monzodioritic rocks have higher liquidus than the granitic rocks.

The melt viscosity models for the mingling- and mixing-related rocks devised by Fred (2017) were tested and the conclusions drawn from the models are applicable also with the temperature results from the geothermobarometry from this study. This supports the results of the study and motivates future research of rock types related to the magma interaction structures. The role of H_2O in the mixing process has been evaluated and tested by Fred (2017) in the viscosity models but remains unconstrained. Salonsaari (1995) proposed that the amount of fluorine in melts has similar effect on the rheological properties of the magma as H_2O. The high F content in the mafic magma of the Jaala-Iitti complex indicates that it possibly lowered the solidus temperature of the mafic magma and increased the time when two contrasting magmas were able to interact. The high F content and its relation to viscosity could give more answers also for the magma interaction of the Ahvenisto complex.

REFERENCES

Ague, J.J. 1997. Thermodynamic calculation of emplacement pressures for batholithic rocks, California: Implications for the aluminum-in-hornblende barometer. Geology 25 (6), 563–566.

Alviola, R., Johanson, B.S., Rämö, O.T. and Vaasjoki, M. 1999. The Proterozoic Ahvenisto rapakivi granite–massif-type anorthosite complex, southeastern Finland; petrography and U–Pb chronology. Precambrian Research 95, 89–107.

Anderson, J.L., Barth, A.P., Wooden, J.L and Mazdab, F. 2008 Thermometers and Thermobarometers in Granitic Systems. Reviews in Mineralogy and Geochemistry 69, 121–142.

Bergman, L. 1986. Structure and mechanism of intrusion of postorogenic granites in the archipelago of southwestern Finland. Acta Acad Aboensis Ser B 46 (5), 74 p.

Blundy, J.D. and Holland, T.J.B. 1990. Calcic amphibole equilibria and a new amphibole-plagioclase geothermometer. Contributions to Mineralogy and Petrology 104, 208–224.

Charlier, B., Namur, O., Bolle, O., Latypov, R. and Duchesne, J.C. 2014. Fe-Ti-V-P ore deposits associated with Proterozoic massif-type anorthosites and related rocks. Earth-Science Reviews 141, 56–81.

Eklund, O. 1991. Betydelsen av magmamixing som magmatisk evolutions process i tolkningen av post- och anorogena bergarters uppkomst, Åland sv Finland. Master's Thesis, Åbo Akademi University.

Eklund, O., Fjördö, S. and Lindbeg, B. 1993. Magma mixing, the petrogenetic link between anorthositic suites and rapakivi granites, Åland, SW Finland. Mineralogy and Petrology 47, 705–730.

Elliott, B.A. 2001. Crystallization conditions of the Wiborg rapakivi batholith, SE Finland: an evaluation of amphibole and biotite mineral chemistry. Contributions to Mineralogy and Petrology 72, 305–324.

Emslie, R.F. 1978. Anorthosite massifs, rapakivi granites, and Late Proterozoic drifting in North America. Precambrian research 7, 61–98.

Emslie, R.F., Hamilton, M.A. and Thériault, R.J. 1994. Petrogenesis of a Mid-Proterozoic Anorthosite-Mangerite-Charnockite- Granite (AMCG) Complex: Isotopic and Chemical Evidence from the Nain Plutonic Suite. The Journal of Geology 102, 539-558.

Fonarev, V. I. and Graphchikov, A. A. 1982: Experimental study of Fe-Mg- and Ca-distribution between coexisting ortho- and clinopyroxenes at P=294 MPa, T=750 and 800 oc. Contributions to Mineralogy and Petrology 79, 311–318.

Fred, R. 2017. Mafic and felsic magma interaction in the 1.64 Ga Ahvenisto complex, southeastern Finland: field relations, petrography, geochemistry, and melt viscosity modeling of monzodioritic and granitic rocks. Masther's thesis, Helsinki university, Department of Geosciences and Geography.

Fred, R., Heinonen, A. and Heikkilä, P. 2019. Tracing the styles of mafic-felsic magma interaction: A case study from the Ahvenisto igneous complex, Finland. Advance online publication of the Bulletin of the Geological Society of Finland.

Fred, R., Heinonen, A. and Heinonen, J.S. 2020. Equilibrium crystallization of massif-type anorthosite residual melts: a case study from the 1.64 Ga Ahvenisto complex, Southeastern Finland. Contributions to Mineralogy and Petrology.

Heinonen, A. 2012. Isotopic evidence for the origin of Proterozoic massif-type anorthosites and their relation to rapakivi granites in southern Finland northern Brazil. Unigrafia. Helsinki, Finland.

Heinonen, A.P., Andersen T. and Rämö, O.T. 2010a. Re-evaluation of rapakivi petrogenesis: source constraints from the Hf isotope composition of zircon in the rapakivi associated mafic rocks of southern Finland. Journal of Petrology 51, 1687–1709.

Heinonen, A., Kivisaari, H. and Michallik, R.M. 2019. High-aluminum orthopyroxene megacrysts (HAOM) in the Ahvenisto complex, SE Finland, and the polybaric crystallization of massif-type anorthosites. Contributions to Mineralogy and Petrology 175, 10.

Heinonen, A.P., Rämö, O.T., Mänttäri, I., Johanson B. and Alviola, R. 2010b. Formation and fractionation of High-Al tholeiitic magmas in the Ahvenisto rapakivi granite–massiftype anorthosite complex, southeastern Finland. The Canadian Mineralogist, 48, 969–990.

Heinonen, A., Andersen, T. and Rämö, O.T. and Whitehouse, M.J. 2015. The source of Proterozoic anorthosite and rapakivi granite magmatism: evidence from combined in situ Hf-O isotopes of zircon in the Ahvenisto complex, southeastern Finland. Journal of the Geological Society 172, 103–112.

Holland, T. and Blundy, J.1994. Non-ideal interactions in calcic amphiboles and their bearing on amphibole-plagioclase thermometry. Contributions to Mineral Petrol 116, 433–447

Hollister, L.S., Grissom, G.C., Peters, E.K., Stowell, H.H. and Sisson, V.B. 1987. Confirmation of the empirical correlation of Al in hornblende with pressure of solidification of calc-alkaline plutons. American Mineralogist 72, 231–239.

Johanson, B.S. 1984. Ahvenisto gabbro-anortositkomplex- En petrografisk och mineralogisk undersökning. Helsingfors universitet, Helsinki, Finland.

Kivisaari, H. 2015. High-aluminum orthopyroxene megacrysts (HAOM) and the polybaric crystallization of the Ahvenisto anorthosite. Master's thesis, Helsinki university, Department of Geosciences and Geography.

Leake, B.E. 1978. Nomenclature of amphiboles. Canadian Mineralogist 16, 501–520.

Le Bas, M.J. and Streckeisen, A.L. 1991. The IUGS systematics of igneous rocks. Journal of the Geological Society of London 148, 825–833.

Lindberg, B. and Eklund, O. 1988. Interactions between basaltic and granitic magmas in a Svecofennian postorogenic granitoid intrusion, Aland, southwest Finland. Lithos 22, Elsevier, Amsterdam, Netherlands, 13–23.

Lindsley, D.H. 1983. Pyroxene thermometry. American Mineralogist 68, 477–493.

Lindsley, D.H. and Andersen, D.J. 1983. A two-pyroxene thermometer. Journal of Geophysical Research 88, 887–906.

Marshall, L.A. and Sparks, R.S.J. 1984. Origin of some mixed-magma and net-veined ring intrusions. Journal of Geological Society 141, 171–182.

Mercier, J-C.C., Benoit, V. and Girardeau, J. 1984. Equilibrium state of diopside-bearing harzburgites from ophiolites: geobarometric and geodynamic implications. Contributions to Mineralogy and Petrology 85, 391–403.

Morimoto, N. 1988. Nomenclature of pyroxenes. American Mineralogist 73, 1123–1133.

Pouchou, J.L. and Pichoir, F. 1986. Basic expression of "PAP" computation for quantitative EPMA. In: Brown, J.D. & Packwood, R.H. (eds.) 11 th international Congress on X - ray Optics and Microanalysis (ICXOM), 249–253.

Putirka, K.D. 2008. Thermometers and Barometers for Volcanic Systems. Reviews in Mineralogy & Geochemistry 69, 61–120

Putirka, K. 2016. Amphibole thermometers and barometers for igneous systems and some implications for eruption mechanisms of felsic magmas at arc volcanoes. American Mineralogist 101(4), 841–858.

Rietmeijer, F. J. M. 1984. Pyroxene (re-)equilibration in the Precambrian terrain of SW Norway between 1030–990 Ma and reinterpretation of events during regional cooling (M3 stage). Norsk geologisk tidsskrift l.

Rämö. O.T. 1991. Petrogenesis of Proterozoic rapakivi granites and related basic rocks of southeastern Fennoscandia: Nd and Pb isotopic and general geochemical constraints. Geological Survey of Finland, Bulletin 355.

Rämö, O.T. and Haapala, I. 1995. One hundred years of rapakivi granite. Mineralogy and Petrology 52, 129–185.

Rämö, O.T. and Haapala, I. 2005. Rapakivi granites. In Lehtinen, M., Nurmi, P.A. and Rämö, O.T. Precambrian Geology of Finland-Key to the evolution of the fennoscandian Shield. Elsevier, Amsterdam, Netherlands, 533–562.

Salonsaari, P.T. 1995. Hybridization in the subvolcanic Jaala-Iitti complex and its petrogenetic relation to rapakivi granites and associated mafic rocks of southeastern Finland. Bulletin of the Geological Society of Finland 67.

Savolahti, A. 1956. The Ahvenisto massif in Finland. Bulletin of the Geological Society of Finland 222, 173–197.

Severin, K.P. 2014. Energy Dispersive Spectrometry of Common Rock Forming Minerals. Springer, Netherlands, 225 p.

Sparks, R.S.J. and Marshall, L.A. 1986. Thermal and mechanical constraints on mixing between mafic and silicic magmas. Journal of volcanology and Geothermal Research 29, 99–124.

Vorma, A. 1976. On the petrochemistry of rapakivi granites with special reference to the Laitila massif, southwestern Finland. Geological Survey of Finland. Bulletin 285, 98 p.

Walker, G.P.L. and Skelhorn, R.R. 1966. Some associations of acid and basic igneous rocks. Earth-Science Reviews 2, 93–109.

Wells, P.R.A. 1977. Pyroxene Thermometry in Simple and Complex Systems. Contributions to Mineralogy and Petrology 62, 129–139.

Wiebe, R.A. 1996. Mafic-silicic layered intrusions: the role of basaltic injections on mahmatic processes and the evolution of silicic magma chambers. Transactions of the Royal Society of Edinburgh: Earth Sciences, 87, 233–242.

Wood, B.J. and Banno, S. 1973. Garnet-Orthopyroxene and Orthopyroxene-Clinopyroxene Relationships in Simple and Complex Systems. Contributions to Mineralogy and Petrology 42, 109–124.

APPENDICES

Appendix 1. SAMPLE LOCATION COORDINATE POINTS

Sample ID	Rock type	Study area	X	Y
APHE-14-011.5.H1	Mingling contact	Pärnäjärvi	474212	6788825
APHE-14-011.5.H3	Leucogranite	Pärnäjärvi	474212	6788825
APHE-14-011.E.H1	Monzodiorite pillow	Pärnäjärvi	474212	6788825
RMF-15-112-A.H1	Monzodiorite pillow	Pärnäjärvi	474062	6788337
RMF-15-115-A.H1	Mixing contact	Pärnäjärvi	473987	6788249
RMF-15-115-B.H1	Hornblende granite	Pärnäjärvi	473987	6788249
RMF-15-115-C.H1	Hybrid	Pärnäjärvi	473987	6788249
RMF-18-007-A	Hornblende granite	Tuuliniemi	470353	6805839
RMF-18-013-A	Monzodiorite	Tuuliniemi	470324	6805646
RMF-18-077-A	Monzodiorite	Pökölä	473721	6791083
RMF-18-078-A	Mingling	Pökölä	473750	6791047
RMF-18-110-A	Mingling	Iso Kuoppalampi	472250	6788316
RMF-18-118-C	Monzodiorite	Iso Kuoppalampi	472289	6788626
RMF-18-252-A	Monzodiorite	Iso Kuoppalampi	471431	6788431
RMF-18-168-A	Monzodiorite	Eastern part	482389	6800259
RMF-18-188-A	Monzodiorite	Eastern part	482545	6799288

Coordinates in ETRS-TM35FIN

Appendix 2a. ELECTRON MICROPROBE ANALYSES OF PLAGIOCLASES OF THE AHVENISTO COMPLEX

INTERACTION TYPE OR LOCATION		Mixing Contact	Mixing Contact	Mixing Contact	Mixing Contact	Mixing Contact	Mixing Contact	Mixing Contact	Mixing Contact	Mixing Contact	Mixing Contact	Mixing Hornblede-granite	Mixing Hornblede-granite
SAMPLE		115-A	115-A	115-A	115-A	115-A	115-A	115-A	115-A	115-A	115-A	115-B	115-B
GRAIN		1	1	1	1	1	1	2	2	2	2	1	1
wt%													
	SiO_2	60.26	59.82	61.00	60.34	58.61	58.01	58.50	58.99	59.11	59.00	61.39	59.92
	Al_2O_3	24.60	24.86	24.28	24.78	25.81	25.96	25.41	25.18	24.98	25.40	23.99	24.69
	TiO_2	0.03	0.06	0.06	0.02	0.04	0.07	0.03	0.04	0.04	0.06	0.00	0.01
	FeO^{tot}	0.13	0.24	0.11	0.13	0.14	0.16	0.11	0.08	0.10	0.07	0.12	0.16
	MgO	0.00	0.01	0.00	0.01	0.02	0.00	0.00	0.00	0.00	0.00	0.02	0.01
	CaO	6.48	6.76	5.96	6.47	7.83	7.93	7.49	7.33	7.10	7.43	5.90	6.72
	Na_2O	7.98	7.75	8.36	8.00	7.16	7.10	7.43	7.45	7.51	7.44	8.33	7.78
	K_2O	0.37	0.31	0.28	0.30	0.31	0.28	0.21	0.19	0.21	0.24	0.39	0.46
	BaO	0.00	0.00	0.00	0.00	0.03	0.01	0.00	0.00	0.00	0.00	0.00	0.00
Total		99.85	99.80	100.04	100.05	99.94	99.52	99.19	99.25	99.06	99.65	100.15	99.75
Formula based on 8 oxygen atoms													
	Si	2.69	2.68	2.71	2.69	2.62	2.61	2.64	2.65	2.66	2.64	2.73	2.68
	Al	1.29	1.31	1.27	1.30	1.36	1.38	1.35	1.34	1.33	1.34	1.26	1.30
	Ti	0.00	0.00	0.00	0.00	0.00	0.00	0.00	0.00	0.00	0.00	0.00	0.00
	Fe^{tot}	0.00	0.01	0.00	0.00	0.01	0.01	0.00	0.00	0.00	0.00	0.00	0.01
	Mg	0.00	0.00	0.00	0.00	0.00	0.00	0.00	0.00	0.00	0.00	0.00	0.00
	Ca	0.31	0.32	0.28	0.31	0.38	0.38	0.36	0.35	0.34	0.36	0.28	0.32
	Na	0.69	0.67	0.72	0.69	0.62	0.62	0.65	0.65	0.66	0.65	0.72	0.68
	K	0.02	0.02	0.02	0.02	0.02	0.02	0.01	0.01	0.01	0.01	0.02	0.03
	Ba	0.00	0.00	0.00	0.00	0.00	0.00	0.00	0.00	0.00	0.00	0.00	0.00
Total		5.01	5.01	5.01	5.01	5.01	5.01	5.02	5.01	5.00	5.01	5.01	5.01
X_{an}		0.303	0.319	0.278	0.303	0.370	0.376	0.353	0.348	0.339	0.351	0.275	0.315
X_{ab}		0.676	0.663	0.706	0.680	0.613	0.609	0.635	0.641	0.649	0.636	0.703	0.660
X_{or}		0.021	0.018	0.016	0.017	0.017	0.016	0.012	0.011	0.012	0.014	0.022	0.026

FeO^{tot} & Fe^{tot} = Total iron

Mixing	Mixing	Mixing	Mixing	Mixing	Mixing	Mingling	Mingling	Mingling	Mingling	Mingling	Mingling	Mingling	Mingling	Mingling
Hornblede-granite	Hornblede-granite	Hybrid	Hybrid	Hybrid	Hybrid	Pillow	Pillow	Pillow	Pillow	Leuco-granite	Leuco-granite	Leuco-granite	Leuco-granite	Contact
115-B	115-B	115-C	115-C	115-C	115-C	011.E	011.E	011.E	011.E	011.5.H3	011.5.H3	011.5.H3	011.5.H3	011.5.H1
2	2	1	1	2	2	1	1	2	2	1	1	2	2	1
61.79	61.94	58.22	57.68	60.73	60.34	53.68	53.07	53.50	53.30	61.28	62.57	61.74	62.54	53.57
23.83	23.85	25.98	26.12	24.61	24.24	28.04	28.09	28.62	27.80	23.42	23.66	23.60	23.08	28.71
0.02	0.02	0.08	0.05	0.02	0.01	0.09	0.09	0.07	0.10	0.01	0.00	0.00	0.02	0.06
0.14	0.10	0.17	0.15	0.16	0.16	0.25	0.27	0.15	0.17	0.13	0.10	0.08	0.04	0.28
0.00	0.00	0.01	0.00	0.02	0.02	0.02	0.02	0.01	0.02	0.04	0.01	0.02	0.02	0.08
5.66	5.77	8.21	8.36	6.50	6.59	11.19	11.35	11.50	11.38	5.08	5.10	5.32	4.52	11.35
8.45	8.42	6.87	6.74	7.93	7.89	4.80	4.85	4.90	4.86	8.53	8.64	8.59	9.03	4.97
0.34	0.33	0.41	0.40	0.35	0.30	0.25	0.22	0.16	0.16	0.45	0.43	0.30	0.39	0.20
0.01	0.00	0.07	0.02	0.01	0.01	0.01	0.00	0.00	0.00	0.00	0.00	0.00	0.00	0.00
100.23	100.43	100.01	99.52	100.32	99.57	98.32	97.97	98.90	97.78	98.93	100.52	99.65	99.65	99.23
2.74	2.74	2.61	2.60	2.70	2.70	2.46	2.45	2.44	2.46	2.75	2.76	2.75	2.78	2.44
1.25	1.24	1.37	1.39	1.29	1.28	1.52	1.53	1.54	1.51	1.24	1.23	1.24	1.21	1.54
0.00	0.00	0.00	0.00	0.00	0.00	0.00	0.00	0.00	0.00	0.00	0.00	0.00	0.00	0.00
0.01	0.00	0.01	0.01	0.01	0.01	0.01	0.01	0.01	0.01	0.00	0.00	0.00	0.00	0.01
0.00	0.00	0.00	0.00	0.00	0.00	0.00	0.00	0.00	0.00	0.00	0.00	0.00	0.00	0.01
0.27	0.27	0.39	0.40	0.31	0.32	0.55	0.56	0.56	0.56	0.24	0.24	0.25	0.22	0.55
0.73	0.72	0.60	0.59	0.68	0.69	0.43	0.43	0.43	0.44	0.74	0.74	0.74	0.78	0.44
0.02	0.02	0.02	0.02	0.02	0.02	0.01	0.01	0.01	0.01	0.03	0.02	0.02	0.02	0.01
0.00	0.00	0.00	0.00	0.00	0.00	0.00	0.00	0.00	0.00	0.00	0.00	0.00	0.00	0.00
5.01	5.00	5.01	5.01	5.00	5.01	4.99	5.00	5.00	4.99	5.01	5.00	5.01	5.01	5.01
0.265	0.270	0.389	0.398	0.306	0.311	0.554	0.556	0.559	0.559	0.242	0.240	0.250	0.212	0.552
0.716	0.712	0.588	0.580	0.675	0.673	0.431	0.431	0.431	0.432	0.733	0.736	0.733	0.766	0.437
0.019	0.018	0.023	0.023	0.019	0.017	0.015	0.013	0.009	0.010	0.025	0.024	0.017	0.022	0.012

Mingling Contact 011.5.H1 1	Mingling Contact 011.5.H1 2	Mingling Contact 011.5.H1 2	Eastern part Monzo-diorite 118-A 1	Eastern part Monzo-diorite 118-A 1	Eastern part Monzo-diorite 118-A 1	Eastern part Monzo-diorite 118-A 2	Eastern part Monzo-diorite 118-A 2	Eastern part Monzo-diorite 118-A 2	Pökölä Monzo-diorite 077-A 1	Pökölä Monzo-diorite 077-A 1	Pökölä Monzo-diorite 077-A 1	Pökölä Monzo-diorite 077-A 2	Pökölä Monzo-diorite 077-A 2	Pökölä Monzo-diorite 077-A 2
53.38	63.70	66.51	58.02	57.33	57.53	56.90	56.92	56.74	56.90	57.09	56.67	57.03	57.98	57.75
29.00	22.84	20.71	26.67	26.53	26.70	26.70	26.86	26.66	25.98	26.65	26.74	26.59	26.69	26.29
0.06	0.02	0.00	0.06	0.05	0.04	0.05	0.03	0.04	0.01	0.00	0.06	0.03	0.04	0.09
0.10	0.08	0.04	0.27	0.26	0.23	0.22	0.27	0.20	0.22	0.16	0.16	0.20	0.15	0.14
0.00	0.01	0.00	0.02	0.01	0.06	0.02	0.02	0.00	0.02	0.00	0.00	0.03	0.04	0.03
11.75	4.29	2.09	8.75	8.93	8.99	9.40	9.22	9.35	8.92	9.07	9.15	8.79	8.79	8.83
4.88	9.33	10.63	5.92	5.87	5.85	5.97	5.92	5.81	6.19	6.04	5.99	6.26	6.35	6.23
0.07	0.28	0.19	0.62	0.60	0.63	0.35	0.40	0.41	0.36	0.37	0.38	0.33	0.32	0.34
0.00	0.01	0.00	0.00	0.00	0.00	0.00	0.01	0.00	0.00	0.01	0.00	0.00	0.00	0.00
99.25	100.56	100.16	100.32	99.59	100.04	99.62	99.65	99.21	98.60	99.41	99.17	99.25	100.36	99.70
2.43	2.80	2.92	2.59	2.58	2.58	2.56	2.56	2.56	2.59	2.57	2.56	2.58	2.59	2.59
1.56	1.18	1.07	1.40	1.41	1.41	1.42	1.43	1.42	1.39	1.42	1.42	1.42	1.40	1.39
0.00	0.00	0.00	0.00	0.00	0.00	0.00	0.00	0.00	0.00	0.00	0.00	0.00	0.00	0.00
0.00	0.00	0.00	0.01	0.01	0.01	0.01	0.01	0.01	0.01	0.01	0.01	0.01	0.01	0.01
0.00	0.00	0.00	0.00	0.00	0.00	0.00	0.00	0.00	0.00	0.00	0.00	0.00	0.00	0.00
0.57	0.20	0.10	0.42	0.43	0.43	0.45	0.44	0.45	0.43	0.44	0.44	0.43	0.42	0.43
0.43	0.80	0.90	0.51	0.51	0.51	0.52	0.52	0.51	0.55	0.53	0.53	0.55	0.55	0.54
0.00	0.02	0.01	0.04	0.03	0.04	0.02	0.02	0.02	0.02	0.02	0.02	0.02	0.02	0.02
0.00	0.00	0.00	0.00	0.00	0.00	0.00	0.00	0.00	0.00	0.00	0.00	0.00	0.00	0.00
5.00	5.00	5.00	4.97	4.98	4.98	4.99	4.99	4.98	4.99	4.99	4.99	4.99	4.98	4.98
0.568	0.200	0.097	0.433	0.440	0.442	0.456	0.452	0.459	0.434	0.444	0.448	0.429	0.425	0.431
0.428	0.785	0.893	0.531	0.524	0.521	0.524	0.525	0.517	0.545	0.535	0.530	0.552	0.556	0.550
0.004	0.015	0.010	0.036	0.035	0.037	0.020	0.023	0.024	0.021	0.022	0.022	0.019	0.018	0.019

Pärnä-järvi	Pärnä-järvi	Pärnä-järvi	Pärnä-järvi	Pärnä-järvi	Pärnä-järvi	Pärnä-järvi	Pärnä-järvi	Pärnä-järvi
Monzo-diorite	Monzo-diorite	Monzo-diorite	Monzo-diorite	Monzo-diorite	Monzo-diorite	Monzo-diorite	Monzo-diorite	Monzo-diorite
116-A	116-A	116-A	116-A	116-A	116-A	116-A	116-A	116-A
1	1	2	2	2	3	3	3	3
56.18	56.80	58.64	57.32	59.16	59.47	59.90	59.87	60.36
27.08	26.97	25.99	26.06	25.29	25.62	25.18	24.90	25.02
0.03	0.05	0.03	0.00	0.00	0.05	0.03	0.01	0.00
0.20	0.19	0.11	0.16	0.15	0.17	0.18	0.13	0.15
0.01	0.00	0.01	0.03	0.00	0.01	0.00	0.03	0.01
9.63	9.42	8.07	8.30	7.72	7.00	6.72	6.63	6.61
5.94	6.02	6.85	6.75	7.16	7.30	7.45	7.53	7.66
0.18	0.20	0.19	0.23	0.21	0.30	0.30	0.28	0.29
0.00	0.00	0.00	0.00	0.00	0.00	0.00	0.00	0.00
99.25	99.66	99.89	98.84	99.68	99.92	99.76	99.37	100.09
2.54	2.56	2.62	2.60	2.65	2.65	2.67	2.68	2.68
1.45	1.43	1.37	1.39	1.33	1.35	1.32	1.31	1.31
0.00	0.00	0.00	0.00	0.00	0.00	0.00	0.00	0.00
0.01	0.01	0.00	0.01	0.01	0.01	0.01	0.00	0.01
0.00	0.00	0.00	0.00	0.00	0.00	0.00	0.00	0.00
0.47	0.45	0.39	0.40	0.37	0.33	0.32	0.32	0.31
0.52	0.53	0.59	0.59	0.62	0.63	0.64	0.65	0.66
0.01	0.01	0.01	0.01	0.01	0.02	0.02	0.02	0.02
0.00	0.00	0.00	0.00	0.00	0.00	0.00	0.00	0.00
5.00	4.99	4.99	5.00	4.99	4.99	4.99	4.99	4.99
0.468	0.458	0.390	0.399	0.369	0.340	0.327	0.322	0.317
0.522	0.530	0.599	0.588	0.619	0.642	0.656	0.662	0.666
0.011	0.012	0.011	0.013	0.012	0.017	0.017	0.016	0.017

Appendix 2b. ELECTRON MICROPROBE ANALYSES OF BIOTITES OF THE AHVENISTO COMPLEX

INTERACTION TYPE		Mixing	Mixing	Mixing	Mixing	Mixing	Mixing	Mixing
		Contact	Contact	Contact	Hybrid	Hybrid	Hybrid	Hybrid
SAMPLE		115-A	115-A	115-A	115-C	115-C	115-C	115-C
GRAIN		1	2	3	1	1	2	2
wt%								
	SiO_2	33.31	34.46	34.88	35.62	35.10	35.21	35.51
	Al_2O_3	12.68	12.50	12.96	13.30	12.71	12.83	12.84
	TiO_2	4.68	3.85	4.23	4.73	4.86	4.79	4.64
	FeO^{tot}	32.88	32.14	30.65	26.88	28.41	29.05	29.06
	MnO	0.12	0.14	0.16	0.13	0.17	0.18	0.13
	MgO	2.10	2.76	3.55	4.28	4.83	4.95	4.84
	CaO	0.05	0.07	0.08	3.02	0.02	0.02	0.02
	Na_2O	0.03	0.05	0.05	0.05	0.10	0.06	0.06
	K_2O	8.65	8.47	8.69	7.90	8.95	8.83	8.99
Total		94.50	94.42	95.26	95.92	95.14	95.92	96.09
	FeO*	28.86	27.76	26.90	23.50	25.22	25.76	25.78
	Fe_2O_3*	4.02	4.38	3.76	3.38	3.19	3.29	3.28
Formula based on 22 oxygen atoms								
	Si	5.48	5.62	5.59	5.58	5.59	5.57	5.60
	Al^{IV}	2.46	2.38	2.41	2.42	2.39	2.39	2.39
	Fe^{3+}	0.07	0.00	0.00	0.00	0.02	0.05	0.01
T-site		8.00	8.00	8.00	8.00	8.00	8.00	8.00
	Al^{VI}	0.00	0.03	0.04	0.04	0.00	0.00	0.00
	Ti	0.58	0.48	0.51	0.56	0.59	0.57	0.55
	Fe^{2+}	3.97	3.79	3.61	3.08	3.36	3.40	3.40
	Fe^{3+}	0.43	0.54	0.45	0.40	0.36	0.35	0.38
	Mn	0.02	0.02	0.02	0.02	0.02	0.02	0.02
	Mg	0.51	0.67	0.85	1.00	1.15	1.17	1.14
O-site		5.51	5.52	5.48	5.10	5.48	5.51	5.49
	Ca	0.01	0.01	0.01	0.51	0.00	0.00	0.00
	Na	0.01	0.01	0.02	0.01	0.03	0.02	0.02
	K	1.82	1.76	1.78	1.58	1.82	1.78	1.81
A-site		1.84	1.79	1.81	2.10	1.85	1.80	1.83
	Total	15.35	15.31	15.29	15.20	15.33	15.32	15.32
$Fe^{2+}/(Fe^{2+}+Fe^{3+})$		0.89	0.88	0.89	0.89	0.90	0.90	0.90
$Mg/(Mg+Fe^{2+})$		0.11	0.15	0.19	0.25	0.25	0.26	0.25
Fe/(Fe+Mg)		0.90	0.87	0.83	0.78	0.77	0.77	0.77
Al^{tot}		2.46	2.40	2.45	2.46	2.39	2.39	2.39

FeO^{tot} = Total iron

FeO* & Fe_2O_3* = Recalculated by Bruiyn et al. 1983

Fe = Total Fe

Al^{tot} = Total Al

Mingling Pillow 011.E 1	Mingling Pillow 011.E 1	Mingling Pillow 011.E 2	Mingling Pillow 011.E 2	Mingling Leuco-granite 011.5.H3 1	Mingling Leuco-granite 011.5.H3 1	Mingling Leuco-granite 011.5.H3 2	Mingling Leuco-granite 011.5.H3 2	Mingling Contact Pillow 011.5.H1 1	Mingling Contact Pillow 011.5.H1 1	Mingling Contact Granite 011.5.H1 2	Mingling Contact Granite 011.5.H1 2
36.68	36.96	35.90	35.65	35.49	35.13	34.80	34.54	36.60	36.31	34.93	34.71
13.24	13.26	13.13	13.12	14.65	14.91	14.71	15.19	13.81	13.89	14.61	14.89
4.09	3.96	4.19	4.29	3.93	3.97	4.51	3.71	2.75	2.85	4.06	3.50
20.19	20.54	24.08	23.66	26.26	26.38	26.42	26.34	22.31	22.30	26.36	27.05
0.04	0.07	0.05	0.10	0.34	0.26	0.35	0.34	0.12	0.12	0.30	0.29
10.68	10.62	8.19	8.27	5.52	5.30	5.18	5.39	9.95	10.08	5.68	5.92
0.02	0.02	0.02	0.02	0.03	0.04	0.04	0.12	0.03	0.02	0.06	0.04
0.13	0.15	0.09	0.10	0.09	0.09	0.10	0.08	0.13	0.12	0.08	0.06
8.94	8.92	8.85	9.01	9.02	9.20	8.99	8.82	9.10	9.11	8.72	7.50
94.01	94.51	94.49	94.21	95.32	95.27	95.08	94.55	94.79	94.80	94.79	93.96
17.78	18.04	21.18	20.92	23.65	23.89	24.02	23.65	19.26	19.32	23.61	23.49
2.40	2.51	2.90	2.74	2.61	2.49	2.40	2.69	3.04	2.98	2.75	3.56
5.66	5.68	5.61	5.59	5.57	5.53	5.50	5.48	5.65	5.61	5.52	5.50
2.34	2.32	2.39	2.41	2.43	2.47	2.50	2.52	2.35	2.39	2.48	2.50
0.00	0.00	0.00	0.00	0.00	0.00	0.00	0.00	0.00	0.00	0.00	0.00
8.00	8.00	8.00	8.00	8.00	8.00	8.00	8.00	8.00	8.00	8.00	8.00
0.07	0.08	0.03	0.01	0.28	0.30	0.24	0.33	0.17	0.15	0.24	0.28
0.48	0.46	0.50	0.51	0.47	0.47	0.54	0.45	0.32	0.33	0.48	0.42
2.29	2.32	2.77	2.74	3.10	3.15	3.17	3.14	2.49	2.50	3.12	3.11
0.28	0.29	0.34	0.32	0.31	0.29	0.29	0.32	0.35	0.35	0.33	0.42
0.01	0.01	0.01	0.01	0.04	0.03	0.05	0.05	0.02	0.02	0.04	0.04
2.45	2.43	1.91	1.93	1.29	1.24	1.22	1.28	2.29	2.32	1.34	1.40
5.57	5.59	5.55	5.53	5.49	5.49	5.50	5.55	5.64	5.66	5.55	5.68
0.00	0.00	0.00	0.00	0.01	0.01	0.01	0.02	0.00	0.00	0.01	0.01
0.04	0.04	0.03	0.03	0.03	0.03	0.03	0.02	0.04	0.04	0.02	0.02
1.76	1.75	1.76	1.80	1.81	1.85	1.81	1.79	1.79	1.80	1.76	1.52
1.80	1.80	1.79	1.84	1.84	1.88	1.85	1.83	1.84	1.84	1.79	1.54
15.38	15.38	15.34	15.36	15.33	15.37	15.35	15.39	15.47	15.50	15.34	15.22
0.89	0.89	0.89	0.89	0.91	0.91	0.92	0.91	0.88	0.88	0.90	0.88
0.52	0.51	0.41	0.41	0.29	0.28	0.28	0.29	0.48	0.48	0.30	0.31
0.51	0.52	0.62	0.61	0.73	0.73	0.74	0.73	0.55	0.55	0.72	0.72
2.41	2.40	2.42	2.42	2.71	2.77	2.74	2.84	2.51	2.53	2.72	2.78

Appendix 2c. ELECTRON MICROPROBE ANALYSES OF HORNBLENDES OF THE AHVENISTO COMPLEX

INTERACTION TYPE		Mixing	Mixing	Mixing	Mixing	Mixing	Mixing	Mixing	Mixing
		Contact	Contact	Contact	Contact	Contact	Contact	Contact	Contact
SAMPLE		115-A	115-A	115-A	115-A	115-A	115-A	115-A	115-A
GRAIN		1	1	1	1	2	2	2	2
wt%									
	SiO_2	41.51	41.19	42.56	41.79	41.57	41.20	41.17	41.33
	Al_2O_3	8.62	9.13	7.37	8.50	8.66	8.55	8.59	8.52
	TiO_2	1.36	1.16	1.84	2.11	2.12	2.10	2.08	2.10
	FeO^{tot}	26.76	26.21	26.98	26.11	24.94	25.24	25.53	25.45
	MnO	0.29	0.35	0.44	0.37	0.33	0.34	0.30	0.31
	MgO	4.92	4.99	4.68	5.28	5.64	5.45	5.47	5.39
	CaO	10.21	10.38	10.19	10.14	10.23	10.08	9.94	9.97
	Na_2O	1.75	1.81	1.63	1.83	1.72	1.76	1.70	1.73
	K_2O	1.38	1.35	1.29	1.45	1.44	1.47	1.42	1.45
Total		96.80	96.57	96.98	97.57	96.65	96.20	96.20	96.25
	FeO*	22.75	22.28	22.93	22.19	21.20	21.46	21.70	21.63
	Fe_2O_3*	4.55	4.46	4.59	4.44	4.24	4.29	4.34	4.33
Formula based on 23 oxygen atoms									
	Si	6.56	6.52	6.71	6.53	6.53	6.52	6.52	6.54
	Al^{IV}	1.44	1.48	1.29	1.43	1.47	1.48	1.48	1.46
	Fe^{3+}	0.00	0.00	0.00	0.03	0.00	0.00	0.00	0.00
T-site		8.00	8.00	8.00	8.00	8.00	8.00	8.00	8.00
	Al^{VI}	0.16	0.22	0.08	0.10	0.14	0.12	0.12	0.12
	Ti	0.16	0.14	0.22	0.25	0.25	0.25	0.25	0.25
	Fe^{2+}	3.01	2.95	3.02	2.90	2.79	2.84	2.87	2.86
	Fe^{3+}	0.54	0.53	0.54	0.49	0.50	0.51	0.52	0.51
	Mn	0.04	0.05	0.06	0.05	0.04	0.05	0.04	0.04
	Mg	1.09	1.12	1.08	1.21	1.28	1.24	1.20	1.21
M1,M2,M3 sites		5.00	5.00	5.00	5.00	5.00	5.00	5.00	5.00
	Mg	0.07	0.06	0.02	0.02	0.04	0.05	0.09	0.06
	Ca	1.73	1.76	1.72	1.70	1.72	1.71	1.69	1.69
	Na	0.20	0.18	0.26	0.28	0.24	0.24	0.23	0.25
M4 site		2.00	2.00	2.00	2.00	2.00	2.00	2.00	2.00
	Na	0.34	0.37	0.24	0.27	0.28	0.30	0.29	0.28
	K	0.28	0.27	0.26	0.29	0.29	0.30	0.29	0.29
A-site		0.61	0.64	0.50	0.56	0.57	0.59	0.58	0.57
	Total	15.61	15.64	15.50	15.56	15.57	15.59	15.58	15.57
$Fe^{3+}/(Fe^{2+}+Fe^{3+})$		0.15	0.15	0.15	0.14	0.15	0.15	0.15	0.15
$Mg/(Mg+Fe^{2+})$		0.28	0.29	0.27	0.30	0.32	0.31	0.31	0.31
Al^{tot}		1.60	1.70	1.37	1.53	1.60	1.59	1.60	1.59

FeO^{tot} = Total iron

FeO* & Fe_2O_3* = Recalculated after Fe^{2+} and Fe^{3+} in formula

Al^{tot} = Total Al

Mixing	Mixing	Mixing	Mixing	Mixing	Mixing	Mixing	Mixing
Hornblende-granite 115-B 1	Hornblende-granite 115-B 1	Hornblende-granite 115-B 2	Hornblende-granite 115-B 2	Hybrid 115-C 1	Hybrid 115-C 1	Hybrid 115-C 2	Hybrid 115-C 2
39.77	39.59	39.89	39.42	41.54	41.72	42.18	42.37
9.04	9.02	9.15	9.16	8.73	8.53	8.82	8.87
1.80	1.78	1.74	1.73	2.11	2.09	1.99	1.99
31.55	31.63	31.40	31.43	25.05	25.10	25.44	25.04
0.42	0.40	0.35	0.41	0.29	0.28	0.26	0.28
1.12	1.09	0.82	0.78	5.82	5.65	5.80	5.81
10.25	10.27	10.22	10.38	10.26	10.37	10.29	10.24
1.96	1.87	1.86	1.89	1.72	1.74	1.78	1.82
1.60	1.57	1.57	1.55	1.45	1.43	1.34	1.40
97.52	97.23	97.00	96.75	96.96	96.92	97.91	97.82
26.82	26.89	26.69	26.72	21.29	21.34	21.63	21.28
5.36	5.38	5.34	5.34	4.26	4.27	4.33	4.26
6.41	6.41	6.45	6.41	6.51	6.54	6.54	6.56
1.59	1.59	1.55	1.59	1.49	1.46	1.46	1.44
0.00	0.00	0.00	0.00	0.00	0.00	0.00	0.00
8.00	8.00	8.00	8.00	8.00	8.00	8.00	8.00
0.13	0.13	0.20	0.16	0.12	0.12	0.15	0.18
0.22	0.22	0.21	0.21	0.25	0.25	0.23	0.23
3.62	3.64	3.61	3.63	2.79	2.80	2.80	2.76
0.65	0.65	0.65	0.65	0.50	0.50	0.50	0.50
0.06	0.06	0.05	0.06	0.04	0.04	0.03	0.04
0.27	0.26	0.20	0.19	1.30	1.30	1.28	1.30
4.94	4.95	4.92	4.91	5.00	5.00	5.00	5.00
0.00	0.00	0.00	0.00	0.06	0.02	0.06	0.04
1.77	1.78	1.77	1.81	1.72	1.74	1.71	1.70
0.23	0.22	0.23	0.19	0.22	0.24	0.23	-0.28
2.00	2.00	2.00	2.00	2.00	2.00	2.00	1.45
0.39	0.37	0.35	0.40	0.30	0.29	0.31	0.28
0.33	0.32	0.32	0.32	0.29	0.29	0.26	0.28
0.71	0.69	0.68	0.73	0.59	0.58	0.57	0.56
15.66	15.65	15.59	15.63	15.59	15.58	15.57	15.02
0.15	0.15	0.15	0.15	0.15	0.15	0.15	0.15
0.07	0.07	0.06	0.06	0.33	0.32	0.32	0.33
1.72	1.72	1.74	1.76	1.61	1.58	1.61	1.62

Appendix 2d. ELECTRON MICROPROBE ANALYSES OF ALKALI FELDSPARS OF THE AHVENISTO COMPLEX

INTERACTION TYPE OR LOCATION		Mixing	Mixing	Mixing	Mixing	Mixing	Mixing	Mixing Hornblede-granite	Mixing Hornblede-granite	Mixing Hornblede-granite	Mixing Hornblede-granite	Mixing	Mixing	Mixing	Mixing
		Contact	Contact	Contact	Contact	Contact	Contact					Hybrid	Hybrid	Hybrid	Hybrid
SAMPLE		115-A	115-A	115-A	115-A	115-A	115-A	115-B	115-B	115-B	115-B	115-C	115-C	115-C	115-C
GRAIN		1	1	1	2	2	2	1	1	2	2	1	1	2	2
wt%															
	SiO_2	65.16	65.17	65.31	65.58	65.50	65.10	64.91	65.42	65.42	64.62	65.13	64.86	65.13	64.97
	Al_2O_3	18.64	18.48	18.51	18.41	18.16	18.12	17.84	18.04	18.20	18.14	18.62	18.44	18.04	18.32
	TiO_2	0.00	0.01	0.01	0.00	0.03	0.09	0.03	0.01	0.03	0.02	0.06	0.03	0.00	0.03
	FeO^{tot}	0.06	0.05	0.00	0.02	0.04	0.08	0.03	0.06	0.10	0.06	0.10	0.11	0.09	0.03
	MgO	0.00	0.02	0.02	0.00	0.01	0.01	0.00	0.02	0.00	0.02	0.00	0.00	0.02	0.00
	CaO	0.15	0.12	0.14	0.24	0.11	0.09	0.05	0.06	0.05	0.03	0.12	0.09	0.09	0.09
	Na_2O	2.19	2.03	2.56	1.26	1.57	1.51	0.84	0.75	0.73	0.52	1.63	1.61	0.83	0.79
	K_2O	13.27	13.69	13.24	13.33	14.37	14.47	15.46	15.38	15.59	15.80	14.30	14.11	15.34	15.46
	BaO	0.46	0.50	0.43	0.36	0.40	0.37	0.21	0.27	0.24	0.20	0.48	0.55	0.44	0.49
Total		99.93	100.07	100.22	99.21	100.20	99.86	99.37	100.01	100.37	99.41	100.45	99.80	99.98	100.17
Formula based on 8 oxygen atoms															
	Si	2.99	2.99	2.99	3.02	3.01	3.00	3.01	3.01	3.01	3.00	2.99	2.99	3.01	3.00
	Al	1.01	1.00	1.00	1.00	0.98	0.98	0.98	0.98	0.99	0.99	1.01	1.00	0.98	1.00
	Ti	0.00	0.00	0.00	0.00	0.00	0.00	0.00	0.00	0.00	0.00	0.00	0.00	0.00	0.00
	Fe^{tot}	0.00	0.00	0.00	0.00	0.00	0.00	0.00	0.00	0.00	0.00	0.00	0.00	0.00	0.00
	Mg	0.00	0.00	0.00	0.00	0.00	0.00	0.00	0.00	0.00	0.00	0.00	0.00	0.00	0.00
	Ca	0.01	0.01	0.01	0.01	0.01	0.00	0.00	0.00	0.00	0.00	0.01	0.00	0.00	0.00
	Na	0.20	0.18	0.23	0.11	0.14	0.14	0.08	0.07	0.07	0.05	0.15	0.14	0.07	0.07
	K	0.78	0.80	0.77	0.78	0.84	0.85	0.92	0.90	0.91	0.94	0.84	0.83	0.90	0.91
	Ba	0.01	0.01	0.01	0.01	0.01	0.01	0.00	0.00	0.00	0.00	0.01	0.01	0.01	0.01
Total		4.99	4.99	5.00	4.93	4.99	4.99	4.99	4.98	4.98	4.99	5.00	4.99	4.98	4.99
X_{an}		0.010	0.008	0.009	0.016	0.007	0.006	0.003	0.004	0.003	0.002	0.008	0.006	0.005	0.006
X_{ab}		0.140	0.128	0.161	0.085	0.098	0.094	0.052	0.046	0.045	0.032	0.102	0.102	0.051	0.048
X_{or}		0.850	0.864	0.831	0.899	0.895	0.900	0.945	0.950	0.952	0.966	0.891	0.893	0.944	0.946

FeO^{tot} & Fe^{tot} = Total iron

Appendix 2e. ELECTRON MICROPROBE ANALYSES OF PYROXENES OF THE AHVENISTO COMPLEX

LOCATION		Monzo-diorite Eastern part	Monzo-diorite Eastern part	Monzo-diorite Eastern part	Monzo-diorite Eastern part	Monzo-diorite Eastern part	Monzo-diorite Eastern part	Monzo-diorite Pökölä	Monzo-diorite Pökölä	Monzo-diorite Pökölä
PYROXENE GROUP		OPX	OPX	OPX	OPX	OPX	OPX	OPX	OPX	OPX
SAMPLE		188-A	188-A	188-A	188-A	188-A	188-A	077-A	077-A	077-A
GRAIN		1	1	1	2	2	2	1	1	1
wt%										
	SiO_2	49.46	50.08	50.00	49.27	49.55	49.57	48.98	48.80	48.73
	Al_2O_3	0.66	0.55	0.57	0.50	0.45	0.53	0.39	0.47	0.44
	TiO_2	0.17	0.14	0.18	0.14	0.13	0.16	0.19	0.16	0.14
	FeO^{tot}	34.22	34.48	34.00	33.91	34.62	34.10	38.02	37.14	37.74
	MnO	0.60	0.63	0.64	0.71	0.64	0.61	0.71	0.71	0.67
	MgO	11.90	11.64	11.56	12.07	11.89	11.76	10.44	10.39	10.69
	CaO	2.75	2.45	3.15	2.52	2.53	2.60	0.94	1.10	0.89
	Na_2O	0.01	0.03	0.05	0.04	0.02	0.05	0.00	0.01	0.06
	K_2O	0.00	0.00	0.00	0.00	0.02	0.00	0.02	0.00	0.01
	Cr_2O_3	0.03	0.01	0.00	0.00	0.00	0.00	0.01	0.05	0.01
	NiO	0.03	0.00	0.00	0.00	0.01	0.00	0.02	0.00	0.00
	ZnO	0.06	0.06	0.04	0.08	0.11	0.07	0.05	0.10	0.04
Total		99.88	100.09	100.19	99.25	99.97	99.44	99.76	98.93	99.42
Formula based on 6 oxygen atoms										
	Si	1.97	1.99	1.99	1.98	1.98	1.99	1.98	1.99	1.98
	Al^{IV}	0.03	0.01	0.01	0.02	0.02	0.01	0.02	0.01	0.02
T site		2.00	2.00	2.00	2.00	2.00	2.00	2.00	2.00	2.00
	Al^{VI}	0.01	0.02	0.01	0.00	0.00	0.01	0.00	0.01	0.00
	Fe^{3+}	0.01	0.00	0.00	0.02	0.02	0.00	0.00	0.00	0.02
	Ti	0.01	0.00	0.01	0.00	0.00	0.00	0.01	0.00	0.00
	Cr	0.00	0.00	0.00	0.00	0.00	0.00	0.00	0.00	0.00
	V	0.00	0.00	0.00	0.00	0.00	0.00	0.00	0.00	0.00
	Zn	0.00	0.00	0.00	0.00	0.00	0.00	0.00	0.00	0.00
	Mg	0.71	0.69	0.68	0.72	0.71	0.70	0.63	0.63	0.65
	Fe^{2+}	0.26	0.28	0.30	0.25	0.26	0.28	0.36	0.35	0.33
	Mn	0.00	0.00	0.00	0.00	0.00	0.00	0.00	0.00	0.00
M1		1.00	1.00	1.00	1.00	1.00	1.00	1.00	1.00	1.00
	Mg	0.00	0.00	0.00	0.00	0.00	0.00	0.00	0.00	0.00
	Fe^{2+}	0.87	0.87	0.83	0.87	0.88	0.86	0.93	0.92	0.93
	Mn	0.02	0.02	0.02	0.02	0.02	0.02	0.02	0.02	0.02
	Ca	0.12	0.10	0.13	0.11	0.11	0.11	0.04	0.05	0.04
	Na	0.00	0.00	0.00	0.00	0.00	0.00	0.00	0.00	0.00
M2		1.01	1.00	0.99	1.01	1.01	1.00	0.99	0.99	1.00
	Total	4.00	3.99	3.99	4.00	4.00	4.00	3.99	3.99	4.00
Fe/(Fe+Mg)		0.614	0.624	0.623	0.608	0.616	0.619	0.671	0.667	0.661
XWo		0.059	0.053	0.068	0.054	0.054	0.056	0.021	0.024	0.019
XEn		0.356	0.352	0.348	0.362	0.355	0.355	0.318	0.320	0.325
XFs		0.585	0.595	0.584	0.583	0.591	0.588	0.662	0.655	0.655

FeO^{tot} = Total iron

i = CPX inclusion in OPX

Fe^{2+} & Fe^{3+} = Recalculated from the mineral formula (Droop G.T.R. 1987)

Monzo-diorite Pökölä OPX 077-A 3	Monzo-diorite Pökölä OPX 077-A 3	Monzo-diorite Pökölä OPX 077-A 3	Monzo-diorite Pökölä OPX 077-A 4	Monzo-diorite Pökölä OPX 077-A 4	Monzo-diorite Pökölä OPX 077-A 4	Monzo-diorite Pärnä-järvi OPX 116-A 1	Monzo-diorite Pärnä-järvi OPX 116-A 1	Monzo-diorite Pärnä-järvi OPX 116-A 2	Monzo-diorite Pärnä-järvi OPX 116-A 2	Monzo-diorite Pärnä-järvi OPX 116-A 2	Monzo-diorite Pärnä-järvi OPX 116-A 2	Monzo-diorite Pärnä-järvi OPX 116-A 3
48.96	48.67	48.50	49.42	48.96	49.58	47.78	47.58	48.66	48.48	48.49	48.50	48.73
0.55	0.53	0.52	0.54	0.56	0.55	0.32	0.29	0.34	0.34	0.32	0.31	0.28
0.15	0.15	0.23	0.29	0.17	0.20	0.07	0.08	0.16	0.13	0.13	0.10	0.13
37.12	37.65	37.50	37.32	37.05	36.72	42.15	41.56	39.01	39.11	38.59	38.42	41.62
0.76	0.69	0.70	0.71	0.69	0.64	0.79	0.81	0.73	0.74	0.64	0.72	0.81
10.84	10.54	11.06	10.93	10.88	10.99	7.59	7.57	7.78	7.70	7.61	7.63	7.93
0.96	1.07	1.07	1.31	1.32	1.30	1.20	1.16	3.77	3.60	4.10	4.24	1.15
0.02	0.01	0.02	0.02	0.03	0.03	0.01	0.00	0.03	0.04	0.08	0.06	0.00
0.00	0.00	0.01	0.00	0.01	0.00	0.00	0.00	0.00	0.00	0.00	0.00	0.00
0.00	0.00	0.01	0.00	0.00	0.04	0.00	0.01	0.00	0.00	0.02	0.00	0.00
0.03	0.01	0.02	0.04	0.01	0.00	0.02	0.00	0.00	0.02	0.00	0.01	0.00
0.07	0.05	0.13	0.02	0.01	0.02	0.11	0.06	0.11	0.09	0.05	0.07	0.00
99.46	99.38	99.76	100.60	99.68	100.08	100.02	99.13	100.61	100.25	100.03	100.06	100.66
1.98	1.98	1.96	1.98	1.98	1.99	1.98	1.98	1.98	1.98	1.99	1.99	1.99
0.02	0.03	0.02	0.02	0.02	0.01	0.02	0.02	0.02	0.02	0.01	0.01	0.01
2.00	2.00	1.99	2.00	2.00	2.00	1.99	2.00	2.00	2.00	2.00	2.00	2.00
0.01	0.00	0.00	0.00	0.01	0.01	0.00	0.00	0.00	0.00	0.00	0.00	0.01
0.00	0.01	0.04	0.00	0.01	0.00	0.04	0.02	0.01	0.01	0.01	0.01	0.00
0.00	0.00	0.01	0.01	0.01	0.01	0.00	0.00	0.00	0.00	0.00	0.00	0.00
0.00	0.00	0.00	0.00	0.00	0.00	0.00	0.00	0.00	0.00	0.00	0.00	0.00
0.00	0.00	0.00	0.00	0.00	0.00	0.00	0.00	0.00	0.00	0.00	0.00	0.00
0.00	0.00	0.00	0.00	0.00	0.00	0.00	0.00	0.00	0.00	0.00	0.00	0.00
0.65	0.64	0.67	0.65	0.66	0.66	0.47	0.47	0.47	0.47	0.46	0.47	0.48
0.33	0.34	0.28	0.33	0.32	0.32	0.49	0.51	0.51	0.51	0.51	0.51	0.51
0.00	0.00	0.00	0.00	0.00	0.00	0.00	0.00	0.00	0.00	0.00	0.00	0.00
1.00	1.00	1.00	1.00	1.00	1.00	1.00	1.00	1.00	1.00	1.00	1.00	1.00
0.00	0.00	0.00	0.00	0.00	0.00	0.00	0.00	0.00	0.00	0.00	0.00	0.00
0.93	0.93	0.95	0.92	0.92	0.91	0.93	0.92	0.81	0.81	0.80	0.79	0.91
0.03	0.02	0.02	0.02	0.02	0.02	0.03	0.03	0.03	0.03	0.02	0.02	0.03
0.04	0.05	0.05	0.06	0.06	0.06	0.05	0.05	0.16	0.16	0.18	0.19	0.05
0.00	0.00	0.00	0.00	0.00	0.00	0.00	0.00	0.00	0.00	0.01	0.00	0.00
1.00	1.00	1.02	1.00	1.01	0.99	1.02	1.00	1.00	1.00	1.01	1.01	0.99
4.00	4.01	4.01	4.00	4.00	3.99	4.01	4.01	4.00	4.00	4.00	4.00	4.00
0.658	0.666	0.648	0.657	0.655	0.652	0.752	0.753	0.736	0.738	0.738	0.737	0.746
0.021	0.023	0.023	0.028	0.029	0.028	0.026	0.026	0.083	0.079	0.091	0.093	0.025
0.331	0.321	0.333	0.329	0.330	0.334	0.233	0.235	0.237	0.236	0.234	0.234	0.244
0.648	0.656	0.644	0.642	0.642	0.637	0.740	0.739	0.680	0.685	0.676	0.673	0.731

Monzo-diorite Pärnä-järvi OPX 116-A 3	Monzo-diorite Eastern part CPX 188-A 2	Monzo-diorite Eastern part CPX 188-A 2	Monzo-diorite Eastern part CPX 188-A 2	Monzo-diorite Eastern part CPX 188-A 3	Monzo-diorite Eastern part CPX 188-A 3	Monzo-diorite Eastern part CPX 188-A 3	Monzo-diorite Pökölä CPX 077-A 1	Monzo-diorite Pökölä CPX 077-A 1	Monzo-diorite Pökölä CPX 077-A 1	Monzo-diorite Pökölä CPX 077-A 2	Monzo-diorite Pökölä CPX 077-A 2	Monzo-diorite Pökölä CPX 077-A 2
48.65	51.28	51.13	51.35	50.83	50.77	50.95	50.75	50.90	50.73	50.22	50.20	49.69
0.31	1.22	1.13	1.17	0.57	0.76	0.65	0.88	0.79	1.01	1.29	1.29	1.21
0.09	0.25	0.21	0.25	0.01	0.12	0.03	0.17	0.15	0.22	0.34	0.33	0.31
41.63	15.98	15.92	15.83	16.95	17.41	16.94	17.71	17.53	17.53	17.66	17.56	17.56
0.78	0.25	0.25	0.30	0.31	0.32	0.30	0.29	0.34	0.29	0.31	0.36	0.35
7.69	9.90	9.64	9.65	9.25	9.36	9.08	8.90	8.82	8.79	8.81	8.74	8.75
1.16	21.09	21.39	21.05	20.80	20.66	20.80	20.62	20.55	20.48	20.35	20.31	20.20
0.04	0.16	0.18	0.17	0.17	0.16	0.15	0.22	0.23	0.23	0.22	0.25	0.27
0.00	0.02	0.03	0.00	0.00	0.00	0.01	0.03	0.03	0.03	0.00	0.03	0.00
0.00	0.00	0.00	0.00	0.02	0.00	0.02	0.03	0.01	0.00	0.00	0.00	0.02
0.01	0.04	0.03	0.03	0.01	0.02	0.03	0.01	0.01	0.00	0.01	0.00	0.00
0.06	0.03	0.06	0.00	0.03	0.07	0.01	0.06	0.03	0.02	0.01	0.05	0.03
100.41	100.21	99.96	99.81	98.96	99.64	98.98	99.67	99.40	99.33	99.21	99.11	98.40
1.99	1.97	1.97	1.98	1.99	1.97	1.99	1.98	1.98	1.98	1.96	1.96	1.96
0.01	0.03	0.03	0.02	0.01	0.03	0.01	0.02	0.02	0.02	0.04	0.04	0.04
2.00	2.00	2.00	2.00	2.00	2.00	2.00	2.00	2.00	2.00	2.00	2.00	2.00
0.01	0.02	0.02	0.03	0.01	0.01	0.02	0.02	0.02	0.02	0.02	0.02	0.02
0.00	0.01	0.01	0.00	0.01	0.03	0.00	0.02	0.00	0.00	0.01	0.02	0.03
0.00	0.01	0.01	0.01	0.00	0.00	0.00	0.01	0.00	0.01	0.01	0.01	0.01
0.00	0.00	0.00	0.00	0.00	0.00	0.00	0.00	0.00	0.00	0.00	0.00	0.00
0.00	0.00	0.00	0.00	0.00	0.00	0.00	0.00	0.00	0.00	0.00	0.00	0.00
0.00	0.00	0.00	0.00	0.00	0.00	0.00	0.00	0.00	0.00	0.00	0.00	0.00
0.47	0.57	0.55	0.55	0.54	0.54	0.53	0.52	0.51	0.51	0.51	0.51	0.51
0.51	0.40	0.40	0.41	0.43	0.41	0.45	0.44	0.46	0.46	0.44	0.44	0.43
0.00	0.00	0.00	0.00	0.00	0.00	0.00	0.00	0.00	0.00	0.00	0.00	0.00
1.00	1.00	1.00	1.00	1.00	1.00	1.00	1.00	1.00	1.00	1.00	1.00	1.00
0.00	0.00	0.00	0.00	0.00	0.00	0.00	0.00	0.00	0.00	0.00	0.00	0.00
0.92	0.11	0.10	0.10	0.11	0.13	0.10	0.12	0.11	0.11	0.12	0.12	0.12
0.03	0.01	0.01	0.01	0.01	0.01	0.01	0.01	0.01	0.01	0.01	0.01	0.01
0.05	0.87	0.88	0.87	0.87	0.86	0.87	0.86	0.86	0.86	0.85	0.85	0.85
0.00	0.01	0.01	0.01	0.01	0.01	0.01	0.02	0.02	0.02	0.02	0.02	0.02
1.00	1.00	1.00	0.99	1.00	1.01	0.99	1.01	1.00	0.99	1.00	1.00	1.01
3.99	4.00	4.00	3.99	4.00	4.01	4.00	4.00	4.00	4.00	4.00	4.00	4.01
0.752	0.473	0.476	0.479	0.501	0.498	0.512	0.518	0.527	0.528	0.523	0.523	0.515
0.026	0.444	0.451	0.447	0.441	0.435	0.444	0.438	0.439	0.439	0.436	0.437	0.436
0.238	0.290	0.283	0.285	0.273	0.274	0.269	0.263	0.262	0.262	0.263	0.262	0.262
0.736	0.267	0.266	0.268	0.286	0.291	0.287	0.299	0.298	0.298	0.301	0.301	0.302

Monzo-diorite Pökölä CPX 077-A 3	Monzo-diorite Pökölä CPX 077-A 3	Monzo-diorite Pökölä CPX 077-A 3	Monzo-diorite Pärnä-järvi CPX 116-A 1	Monzo-diorite Pärnä-järvi CPX 116-A 1	Monzo-diorite Pärnä-järvi CPX 116-A 2	Monzo-diorite Pärnä-järvi CPX 116-A 2	Monzo-diorite Pärnä-järvi CPX 116-A 2	Monzo-diorite Pärnä-järvi CPX 116-A i	Monzo-diorite Pärnä-järvi CPX 116-A i	Monzo-diorite Pärnä-järvi CPX 116-A i
50.71	50.72	50.67	50.04	49.80	50.43	50.70	50.32	49.20	49.37	48.94
0.86	0.90	0.84	0.69	0.70	0.65	0.61	0.64	2.03	1.43	2.55
0.17	0.11	0.18	0.12	0.16	0.12	0.15	0.14	0.41	0.34	0.59
17.92	17.88	17.76	21.46	22.08	22.46	22.38	21.84	22.09	21.94	22.23
0.39	0.35	0.33	0.37	0.42	0.42	0.44	0.44	0.34	0.37	0.36
8.86	8.73	8.73	6.57	6.64	6.64	6.68	6.76	6.80	6.87	6.80
20.17	20.23	20.17	19.45	19.28	19.42	19.50	19.56	18.00	18.88	17.16
0.20	0.22	0.23	0.21	0.22	0.23	0.20	0.23	0.41	0.29	0.51
0.03	0.01	0.02	0.00	0.00	0.00	0.00	0.00	0.24	0.14	0.31
0.00	0.00	0.01	0.03	0.00	0.01	0.00	0.02	0.00	0.00	0.00
0.03	0.00	0.00	0.00	0.00	0.02	0.00	0.00	0.02	0.02	0.03
0.13	0.01	0.06	0.07	0.07	0.10	0.01	0.06	0.06	0.03	0.00
99.47	99.16	99.00	99.02	99.38	100.49	100.67	100.00	99.58	99.68	99.48
1.98	1.98	1.98	1.99	1.98	1.99	1.99	1.99	1.95	1.96	1.94
0.02	0.02	0.02	0.01	0.02	0.01	0.01	0.01	0.05	0.04	0.06
2.00	2.00	2.00	2.00	2.00	2.00	2.00	2.00	2.00	2.00	2.00
0.02	0.02	0.02	0.02	0.01	0.02	0.02	0.02	0.04	0.02	0.06
0.01	0.00	0.00	0.00	0.01	0.01	0.00	0.01	0.04	0.04	0.03
0.01	0.00	0.01	0.00	0.00	0.00	0.00	0.00	0.01	0.01	0.02
0.00	0.00	0.00	0.00	0.00	0.00	0.00	0.00	0.00	0.00	0.00
0.00	0.00	0.00	0.00	0.00	0.00	0.00	0.00	0.00	0.00	0.00
0.00	0.00	0.00	0.00	0.00	0.00	0.00	0.00	0.00	0.00	0.00
0.52	0.51	0.51	0.39	0.39	0.39	0.39	0.40	0.21	0.41	0.40
0.44	0.46	0.46	0.57	0.57	0.58	0.58	0.57	0.69	0.52	0.49
0.00	0.00	0.00	0.00	0.00	0.00	0.00	0.00	0.00	0.00	0.00
1.00	1.00	1.00	1.00	1.00	1.00	1.00	1.00	1.00	1.00	1.00
0.00	0.00	0.00	0.00	0.00	0.00	0.00	0.00	0.00	0.00	0.00
0.13	0.12	0.12	0.14	0.15	0.15	0.15	0.14	0.19	0.17	0.21
0.01	0.01	0.01	0.01	0.01	0.01	0.01	0.01	0.01	0.01	0.01
0.84	0.85	0.85	0.83	0.82	0.82	0.82	0.83	0.76	0.80	0.73
0.02	0.02	0.02	0.02	0.02	0.02	0.01	0.02	0.03	0.02	0.04
1.00	1.00	1.00	1.00	1.00	1.00	1.00	1.00	1.00	1.01	0.99
4.00	4.00	4.00	3.99	4.00	4.00	4.00	4.00	4.00	4.01	3.99
0.527	0.534	0.533	0.647	0.647	0.651	0.653	0.642	0.634	0.628	0.637
0.431	0.434	0.434	0.426	0.418	0.417	0.418	0.422	0.400	0.412	0.388
0.263	0.261	0.262	0.200	0.200	0.199	0.199	0.203	0.210	0.208	0.214
0.306	0.305	0.304	0.374	0.381	0.384	0.382	0.375	0.389	0.380	0.399